


5-2014

Broadband Nanostructured Antireflection Coating for Enhancing InAs/GaAs Quantum Dots Solar Cells Performance

Jony C. Sarker

University of Arkansas, Fayetteville

Follow this and additional works at: <http://scholarworks.uark.edu/etd>

 Part of the [Nanoscience and Nanotechnology Commons](#), [Nanotechnology Fabrication Commons](#), and the [Power and Energy Commons](#)

Recommended Citation

Sarker, Jony C., "Broadband Nanostructured Antireflection Coating for Enhancing InAs/GaAs Quantum Dots Solar Cells Performance" (2014). *Theses and Dissertations*. 2334.
<http://scholarworks.uark.edu/etd/2334>

Broadband Nanostructured Antireflection Coating for
Enhancing InAs/GaAs Quantum Dots Solar Cells Performance

Broadband Nanostructured Antireflection Coating for
Enhancing InAs/GaAs Quantum Dots Solar Cells Performance

A thesis submitted in partial fulfillment
of the requirements for the degree of
Master of Science in Electrical Engineering

by

Jony Chandra Sarker
Bangladesh University of Engineering and Technology
Bachelor of Science in Electrical and Electronic Engineering, 2011

May 2014
University of Arkansas

This thesis is approved for recommendation to the Graduate Council.

Dr. Omar Manasreh
Thesis Director

Dr. Simon Ang
Committee Member

Dr. Jingxian Wu
Committee Member

ABSTRACT

The broadband suppression in reflection is one of the primary focuses in high efficiency solar cell research. In this thesis, a moth-eye inspired nanostructure antireflection coating is fabricated on InAs/GaAs quantum dots solar cell in order to enhance the power conversion efficiency. The abrupt refractive index transition between air and GaAs surface is replaced by a tapering zinc oxide nanoneedle on planar tantalum pentoxide coating. The antireflection structure provides gradual reduction of refractive index away from the solar cell top surface.

The nanostructured antireflection coating is fabricated by utilizing chemical bath deposition of tapered zinc oxide nanoneedles on planar tantalum pentoxide coating. A sol-gel method was developed to obtain an air stable tantalum pentoxide solution. The thickness of the planar tantalum pentoxide coating was optimized to suppress the reflection at a single wavelength. In addition, hydrothermally grown zinc oxide nanoneedle arrays were optimized by investigating several growth parameters including pH and growth time to obtain a tapered dimension. A tapering zinc oxide nanoneedle structure coupled with a high refractive index tantalum pentoxide layer suppresses the broadband reflectance to less than 1 %.

The combined antireflection structure significantly increased the performance, not only in reflectance or transmission spectrum, but also in current-voltage characteristic, external quantum efficiency, and spectral response measurements. A power conversion efficiency enhancement of 30 % was obtained by a single quarter wavelength tantalum pentoxide layer. Adding the tapered zinc oxide nanoneedles on top of the planar tantalum pentoxide layer, the power conversion efficiency enhanced by 50 %. Furthermore, a 60 % enhancement in the external quantum efficiency is obtained for the same wavelength range.

ACKNOWLEDGEMENTS

First of all, I would like to express my deep gratitude to my graduate advisor and thesis director, Dr. Omar Manasreh for providing me an opportunity to do this research project. In particular, he laid the foundation for my work on quantum dot solar cells, nanostructure antireflection coating and every experimental result in this thesis bears a trace of his influence. His cheer and charisma, passion and compassion, together make him the most inspiring scientific communicator and leader I know. Without his support it would not have been possible for me to complete this project.

I am thankful to Dr. Simon Ang and Dr. Jingxian Wu for being in my thesis committee.

I am deeply indebted to all past and current group members for establishing the lab, shaping its culture for an excellent research environment. Especially, I wish to thank my group members Yahia Makableh, Ramesh Vasani, Seung Yung Lee, Ahmad Nusir, Dr. M. Alam Khan and Rick Eyi for their constant support and wisdom in completing this project.

I would like to thank Dr. Shui-Qing Yu for providing the facilities in the ellipsometry measurements.

I owe one final acknowledgment to my wife and mother, whose love and support will never flag or fail.

This work was partially supported by the Air Force Office of Scientific Research (Grant FA9550-10-1-0136), the NSF-EPSCoR program (Grant EPS-1003970), and NASA-EPSCoR program (Grant 242026-1/NNX11AQ36A).

TABLE OF CONTENTS

1. INTRODUCTION.....	1
1.1. Thesis Overview.....	1
1.2. Basic of Antireflection coating.....	2
1.3. Moth’s eye inspired nanostructure antireflection coating.....	3
1.4. Nanostructure antireflection coating current progress and limitations	5
2. MATERIALS GROWTH AND DEVICE FABRICATION.....	6
2.1. Introduction.....	6
2.2. Synthesis of tantalum pentoxide sol-gel method.....	6
2.3. Synthesis of zinc oxide nanoneedle by chemical bath deposition process.....	8
2.3.1. Zinc oxide nanoneedle growth , pH and time control	9
2.4. Fabrication of InAs/GaAs Quantum dots solar cells	11
2.4.1. Sample cleaning	11
2.4.2. Photolithography.....	12
2.4.3. Metallization and Lift off	12
3. CHARACTERIZATION TECHNIQUES.....	13
3.1. Material characterization.....	13
3.1.1. Transmission and absorbance measurements	13
3.1.2. Raman Spectroscopy	14
3.1.3. Spectroscopic Ellipsometry	15
3.1.4. Scanning Electron microscope (SEM).....	15
3.2. Device Characterization.....	15
3.2.1. IV Characteristics measurement	16
3.2.2. Quantum Efficiency measurement	17

3.2.3. Spectral Response measurement.....	18
4. RESULTS AND DISCUSSIONS.....	18
4.1. Introduction.....	18
4.2. InAs/GaAs QDs solar cell with antireflection structure.....	19
4.2.1. Antireflection structure characterization	21
4.2.2. Refractive index measurements	23
4.2.3. Reflection and Transmission spectra measurements.....	24
4.2.4. InAs/GaAs quantum dots solar cell device output	27
4.3. Discussions.....	30
5. CONCLUSION AND FUTURE WORK.....	32
5.1. Conclusion.....	32
5.2. Future work.....	32
6. REFERENCES.....	34
Appendix: Associated contribution	38

LIST OF FIGURES

Figure 1.1 Schematic of the reflection of a substrate with a homogeneous planar coating (left) and a nanostructure based graded index refractive index coating (right).....	3
Figure 1.2 Detail image of moth's eye cornea, Inset showing Moth's eye image of a butterfly	4
Figure 2.1 Sol-gel synthesis process is explained in a step by step flow chart.....	7
Figure 2.2 Flow-chart of Ta ₂ O ₅ spin-coating thin film deposition method.....	7
Figure 2.3 Solution preparation flow chart of ZnO nanoneedle growth	8
Figure 2.4 Bilayer antireflection coating of ZnO nanoneedle/ Ta ₂ O ₅ fabrication process flow chart	9
Figure 2.5 Nanoneedles growth of ZnO for zinc nitrite hexahydrate (25 mM) and HMTA (25 mM) and varying the concentration of diaminopropane (DAP) for a) 0 mM b) 190 mM c) 150 mM and d) 120 mM at 85 °C.	10
Figure 2.6 Zinc oxide nanoneedle growth for diaminopropane (DAP) 120 mM in growth solution for a) 120 min. b) 180 min , growth temperature of 85° C.....	11
Figure 3.1 (a) Raman molecular vibration (b) Elastic and inelastic molecular vibration mechanism.....	14
Figure 3.2 A model of current density-voltage (I-V) characteristics for a solar cell in the dark (blue) and under illumination (red).....	16

Figure 4.1 Schematic diagram of a InAs/GaAs QDs solar cell with textured surface of ZnO nanoneedle grown on planar Ta ₂ O ₅	19
Figure 4.2 (a) and (b) A representative cross-section and top view of ZnO nanoneedles grown on top of Ta ₂ O ₅ with scale bar of 1 μm. (c) Scanning electron microscopy (SEM) images of ZnO nanoneedle grown for diaminopropane (DAP) 120 mM in growth solution for 180 min, growth temperature of 85° C with scale bar of 500 nm resolution.....	20
Figure 4.3 Raman spectra of sol-gel derived Ta ₂ O ₅ film, and hydrothermally grown ZnO nanoneedles on Ta ₂ O ₅ film measured at room temperature.....	21
Figure 4.4 Absorbance spectra of solution phase Ta ₂ O ₅ and ZnO nanoneedle measured and compared in wavelength range of 250 – 800nm.....	22
Figure 4.5 Refractive index spectra of GaAs, Ta ₂ O ₅ layer, and ZnO planar coating compared over a range from 400 nm to 870 nm.....	23
Figure 4.6. (a) Reflectance spectra as a function of angle of incidence for GaAs substrate with pristine, Ta ₂ O ₅ , and ZnO nanoneedles surfaces	25
Figure 4.7 Effect of ZnO nanoneedle growth time on specular reflectance spectra for ZnO nanoneedle only (green), bilayer coating of ZnO nanoneedle/Ta ₂ O ₅ , where nanoneedle growth time for 120 minute (blue) and 180 minute (red).....	26
Figure 4.8 Transmission spectra measured for the GaAs substrate with pristine, Ta ₂ O ₅ , and ZnO nanoneedles surfaces.....	27
Figure 4.9 The I-V characteristics measured for the InAs/GaAs QDs solar cell with pristine, Ta ₂ O ₅ , and ZnO nanoneedles surfaces.....	28

Figure 4.10 The external quantum efficiency measured for the InAs/GaAs QDs solar cell with pristine, Ta₂O₅, and ZnO nanoneedles surfaces.....29

Figure 4.11 The Spectral Response measured for the InAs/GaAs QDs solar cell with pristine, Ta₂O₅, and ZnO nanoneedles surfaces.....30

1. INTRODUCTION

The power density of solar radiation incident on the earth's surface is 1.4 kW/m^2 but still scarcely used as stated by the U.S energy information administration (EIA). This coupled with the ever increasing demand on non-conventional sources of energy in the last few decades led to a tremendous boost in the research on enhancing solar cell efficiency [1-5]. Amongst different solar cell materials and structures, InAs quantum dots (QDs) embedded into GaAs p-n junction solar cells has generated much attention due to predicted theoretical power conversion efficiency limit on the order of 63% [4,5]. Specifically, InAs quantum dots (QDs) have three dimensional carrier confinements which increase the absorption of the solar cells below the band gap of the host GaAs material. Hence, this three dimensional carrier confinement makes InAs QDs suitable for high efficiency solar cell applications.

Despite the ability to generate high short-circuit current and open circuit voltage, performance of the InAs QDs solar cell has not reached its theoretical potential, due to high carrier recombination [5] in the QDs and reflection of more than 35 % of incident light from the GaAs top surface [6,7]. In order to improve the performance of the solar cell, several attempts were carried out to reduce the carrier recombination including high density of quantum dots [5], strain compensation technique,[8,9] and energy fence barriers [10]. However, the increase in the device performance still remains negligible. On the other hand, antireflection coatings on InAs/GaAs QDs solar cell can play a major role to significantly improve the device performance.

1.1 Thesis Overview

The motivation behind this thesis was to design and fabricate an antireflection coating to suppress the surface reflection of the top surface of the solar cell in order to utilize the maximum

incident photon. The novel antireflection structure presented in this thesis played a key role in suppressing the reflection by gradual reduction of refractive index away from the GaAs surface. In chapter 1 the basic principle of antireflection coating, current progress and limitation in nanostructure antireflection coating is discussed. Chapters 2 and 3 discuss the synthesis process of planar and nanostructured antireflection coating, solar cell fabrication process and the tools used to characterize them. Chapter 4 analyses the efficiency enhancement of InAs/GaAs quantum dots solar cells by implementing tapered ZnO nanoneedles on planar tantalum pentoxide (Ta₂O₅) coating. Finally, in chapter 5 the project is concluded and the possible future works are proposed.

1.2 Basics of Antireflection coating

A general approach to reduce the reflection from the surface of the solar cell is to design step-down refractive index coating structure (such as $n_s > n_1 > n_2 > n_3 > n_m$) for broadband reflection control [11], where n_s and n_m are refractive index of the substrate and the incident medium respectively. A rule of thumb can be expressed as for N layers of antireflection coating (ARC), for the layer- i refractive index n_i can be obtained as [11],

$$n_i = n_{medium}^{\binom{N+1-i}{N+1}} * n_{cell}^{\binom{i}{N+1}} \dots\dots\dots(1.1)$$

So, if $n_{medium} = air$, then refractive index for each layer can be calculated by

$$n_i = n_{cell}^{\binom{i}{N+1}} \dots\dots\dots(1.2)$$

Multilayer stacks of materials with different refractive indices can be used in order to obtain broadband suppression in reflection. Optimization of multilayer ARC is a difficult challenge because of the large dimensional space of possible solutions to combine each layer [12]. On the

other hand, conically shaped nanostructure provide graded refractive index properties, which can be achieved with low effective refractive index at the top and high effective index at the bottom due to variation of the filling fraction [13]. For example, homogeneous planar coatings reduces the reflection due to interferences of light reflected at the air-to-coating layer interface and at the coating layer -substrate interfaces as shown in Figures. 1.1. For simplicity, only one reflection path is shown which shows multiple reflections occurring in the interface. For the graded refractive index coating which can be obtained by conically shaped nanostructure shows no reflection due to the refractive index matched up at the top and bottom interfaces.

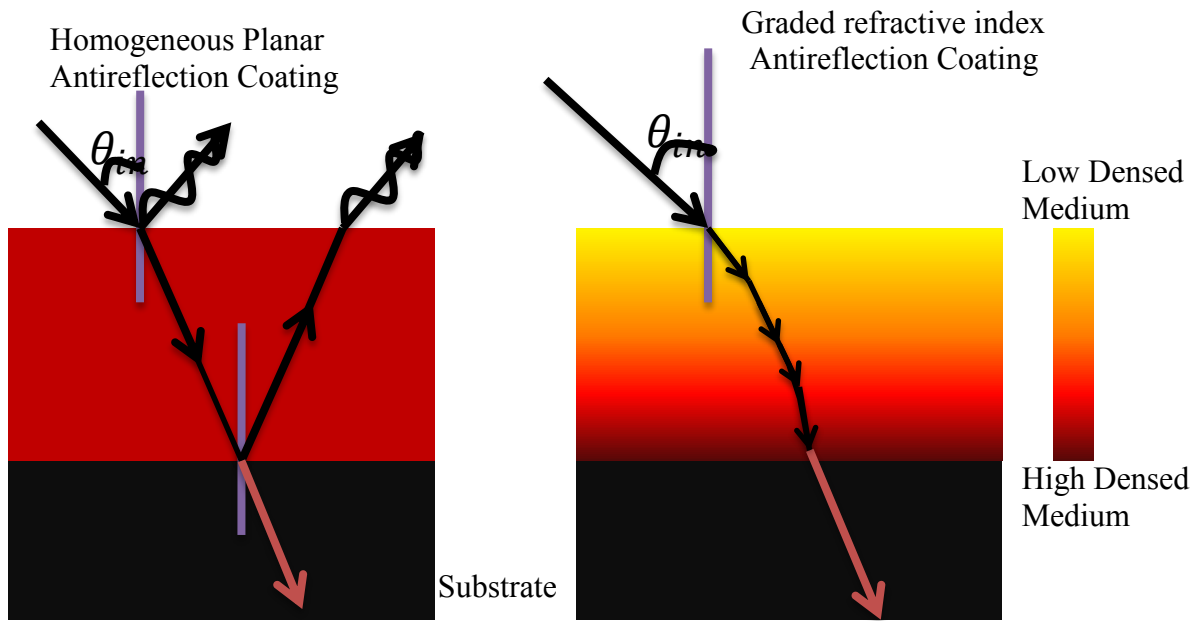


Figure 1.1 Schematic of the reflection mechanism of a substrate with a homogeneous planar coating (left) and a graded index refractive index coating (right).

1.3 Moth’s eye inspired nanostructure antireflection coating

In order to suppress the reflection, several antireflection techniques were carried out including subwavelength structures [14-23], plasmonic surface [24], surface passivation [25],

single quarter wavelength [19], and multilayer coating [26]. Among all these techniques, subwavelength structures emerged as a successful method due to the characteristics of gradual variation of the refractive index or so called moth-eye effect [14,15,17,22,23,13]. The moth-eye effect inspired by the naturally evolved cornea of moth species, which incorporated by nanotip arrays of protuberant structures [17,23] as shown in Figure 1.2. A moth eye antireflection surface is one in which the reflection of incident light is reduced by the presence of a regular array of small protuberances covering the surface. Thus, the surface of the moth-eye's provides gradual decrease of refractive index from their cornea to the surrounding medium in order to suppress the reflection of incident light.

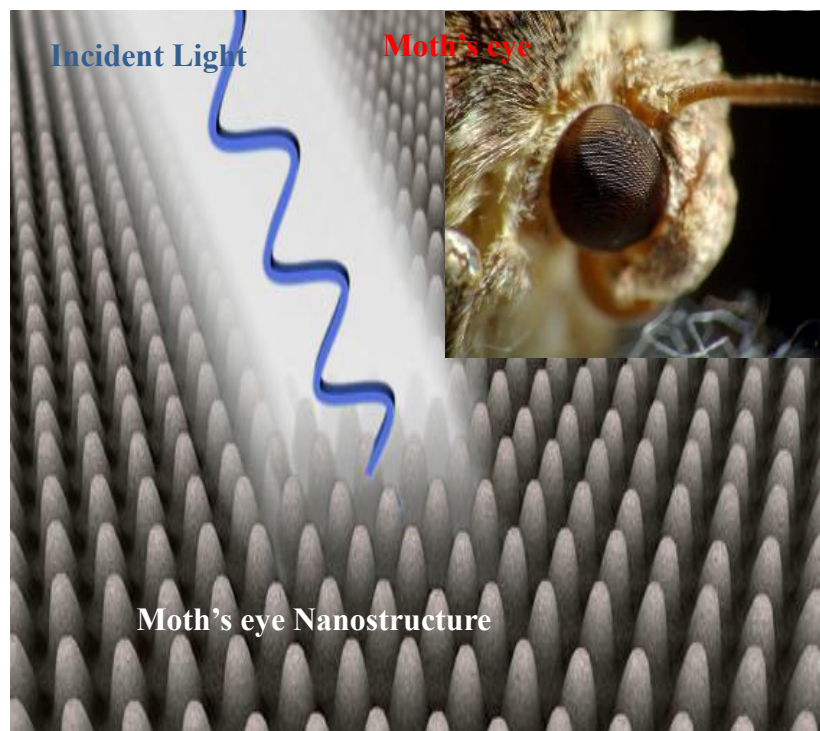


Figure 1.2 Detail image of moth's eye cornea, Inset showing Moth's eye image of a butterfly [15,17,23].

1.4 Nanostructured antireflection coating current progress and limitations

Among the antireflective subwavelength structure fabrication methods, the bottom-up deposition [19-22,26,27] is preferable to its top-down [14,15,17,18,23] counterpart due to simplicity, lithography-free process and economical point of view [19,20,26,28]. Several bottom-up antireflection schemes on GaAs solar cell were reported by using $\text{Si}_3\text{N}_4/\text{SiO}_2/\text{ZnO}$ nanorod [19], indium tin oxide nanocolumns [20], ZnO nanoneedle [28], and TiO_2 /nanoporous SiO_2 [26]. The power conversion efficiency enhancement obtained using these schemes is less than $\sim 35\%$. Despite superior antireflection properties of the reported schemes [19,20,26,28], the coupling of multiple discrete layers by a single deposition process is yet to be achieved. For example, Yan *et al.*[26], Yeh *et al.* [19], and Wu. *et al.* [28]fabricated multilayer antireflection coating (ARC) by incorporating either RF sputtering ,oblique angle electron-beam, or chemical deposition in each layer. On the other hand, Yu. *et al.* [20] reported indium tin oxide nanocolumns using high temperature (above 300°C), usually intolerable in practical solar cell application. On the other hand, ZnO nanostructure arrays synthesized by hydrothermal method hold promising potential due to low growth temperature ($< 90^\circ\text{C}$), high growth rate ($> 1000\text{ nm h}^{-1}$) and lithography-free processes [2,29].

Recently, ZnO nanostructure coupled with a single quarter wavelength coating (reflection minimized for a single wavelength) including Si_3N_4 , and AZO was substantiated by the other researcher [19,27,28] as broadband ARC for the solar cell. A material with refractive indices on the order of $n \sim 2$ [30] such as tantalum pentoxide (Ta_2O_5) can be an alternative for single quarter wavelength coating. Previous investigations on Ta_2O_5 include corrosion protection coating [31], electrochromic devices [32], dielectric spacers for metamaterial, and plasmonic coupler [33,34].An early attempt by electron beam deposition of a single layer Ta_2O_5 coating on silicon

solar cell was reported with an efficiency enhancement on the order of 23 % [35]. However, Ta₂O₅ antireflection coating using sol-gel method limits due to high instability of the sol particle, which originates from fast hydrolysis of tantalum precursor [36,37]. Therefore, sol stabilization is a crucial parameter for the synthesis of Ta₂O₅ antireflection coating. Moreover, ZnO nanostructure coupled with Ta₂O₅ was not implemented so far, which could provide antireflection characteristics beyond the aforementioned performances.

2. MATERIALS GROWTH AND DEVICE FABRICATION

2.1 Introduction

This chapter briefly discuss about the sol-gel synthesis of Ta₂O₅ and hydrothermal growth of ZnO nanoneedle arrays. Then precise control of pH and growth time is discussed to obtain tapered shape ZnO nanoneedle. The last part of this chapter discussed about the fabrication procedure of InAs/GaAs Quantum dots solar cells.

2.2 Synthesis of tantalum pentoxide sol-gel method

The sol-gel method of Ta₂O₅ adapted from Wolf *et al.*[37] and modified by changing the solvent, the ratio between the precursor and hydrolysis component to prevent gelation and obtain a stable Ta₂O₅ solution. The complete sol-gel synthesis process is described in Figure 2.1. The sol-gel was prepared by dissolving (0.53 mL) tantalum (V) ethoxide (Ta(OC₂H₅)₅, 99% pure, Sigma aldrich) in 8 ml methoxy-ethanol 1:50 molar ratio. The precursor in the solvent was stirred for complete dissolution in the solvent. Diethanolamie (DEA) (sigma Aldrich) (0.78 mL) was added drop by drop in the precursor solution and stirred for 2 hours to complete the polymerization reaction. The hydrolysis process was completed by adding DI water (0.23 mL) in

molar ration of 1:10 with the solvent and stirred for half an hour. The molar ration between tantalum ethoxide, DEA and DI water was kept 1:4:5. The pH value of the final transparent sol-gel was 7.5 measured by pH meter. The complete reaction was performed under N₂ environment glove box to prevent the pre-hydrolysis process of the tantalum precursor [44]. A 90 nm thickness Ta₂O₅ single quarter wavelength coating is obtained by spin coating at 6000 rpm and annealed at 150 °C in air for 20 minute as shown in Figure 2.2.

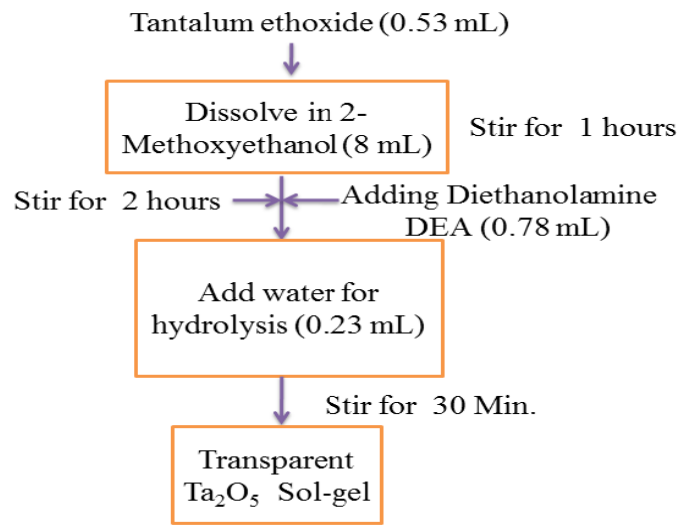


Figure 2.1 Sol-gel synthesis process is explained in a step by step flow chart.

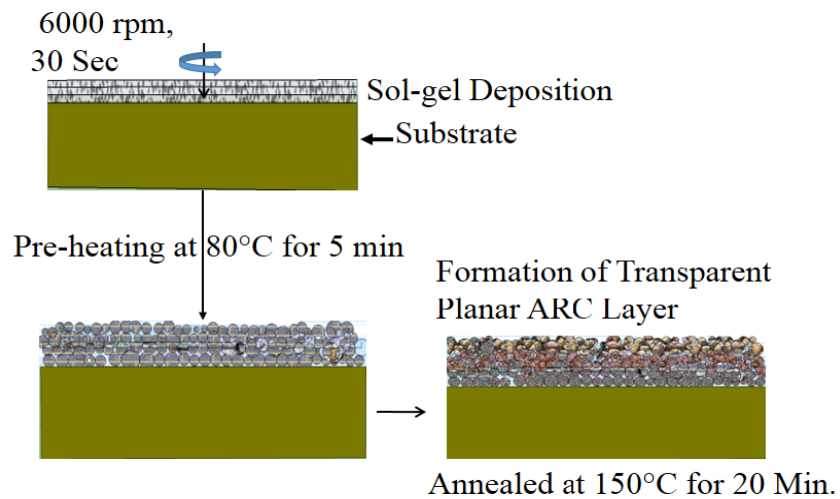


Figure 2.2. Flow-chart of Ta₂O₅ spin-coating thin film deposition method

2.3 Synthesis of Zinc oxide nanoneedle by chemical bath deposition process

The ZnO nanoneedle arrays were grown according to a previously established method [2]. The ZnO seed layer is synthesized from sol-gel and nanoneedle were grown by hydrothermal technique as shown in Figure 2.3. The ZnO sol-gel for seed layer were prepared by mixing 0.3 M zinc acetate dehydrate and 0.3 M ethanolamine in 2-methoxyethanol. The ZnO seed layer on top of Ta₂O₅ coating is obtained by one spin coating cycle at 4000 rpm. The growth solution of ZnO nanoneedle was prepared by 0.025 M solution of zinc nitrate hexahydrate and 0.025 M solution of hexamine in equal volume of DI water. The aqueous bath solutions pH was controlled by adding diaminopropane which adjusted the pH to 12 in the final growth solution [44].

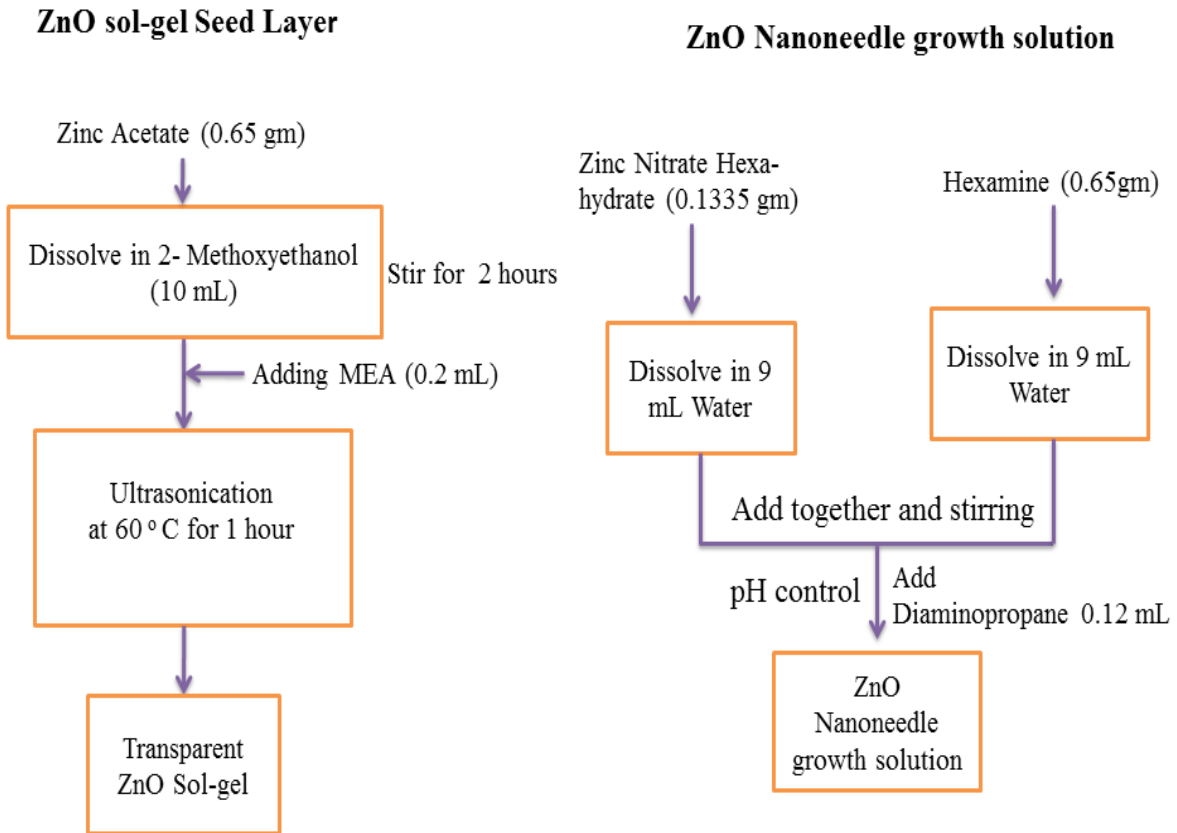


Figure 2.3 Solution preparation flow chart of ZnO nanoneedle growth

To grow the nanoneedle arrays, InAs/GaAs QDs solar cell coated with Ta₂O₅ and ZnO seed layer were placed upside down in the aqueous solution bath at 85 °C. After the growth period of 3 hour, the solar cell was rinsed thoroughly with DI water, dried under nitrogen and annealed in ambient atmosphere at 150 °C. The antireflection structure fabrication procedure is shown in Figure 2.4.

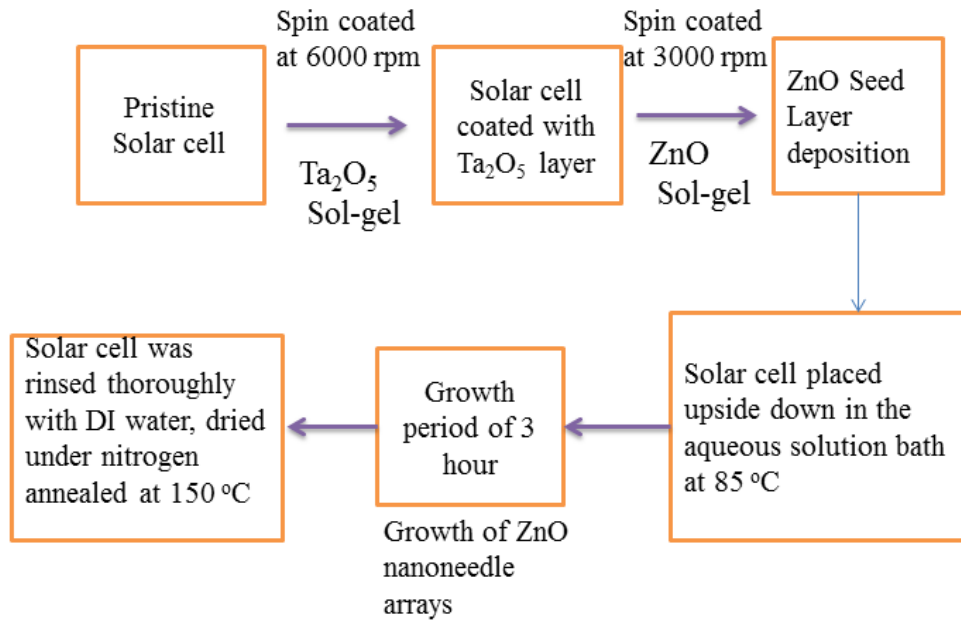


Figure 2.4 Bilayer antireflection coating of ZnO nanoneedle/ Ta₂O₅ fabrication process flow chart

2.3.1 Zinc oxide nanoneedle growth, pH and time control

The pH of the growth solution is adjusted by varying the concentration of diaminopropane (DAP) in the final growth solution in order to obtain the sharp tips. The absence of DAP in the growth solution only results in nanorod as shown in Figure 2.5 (a). The nanoneedle tip strongly depends on the concentration of DAP as shown in Figure 2.5 (b)-(d). At higher concentration of DAP the nanoneedle shows etched tips. The ZnO nanoneedle arrays

without tip etching is obtained by 120 mM DAP concentration and measured pH of the solution was ~ 12 .

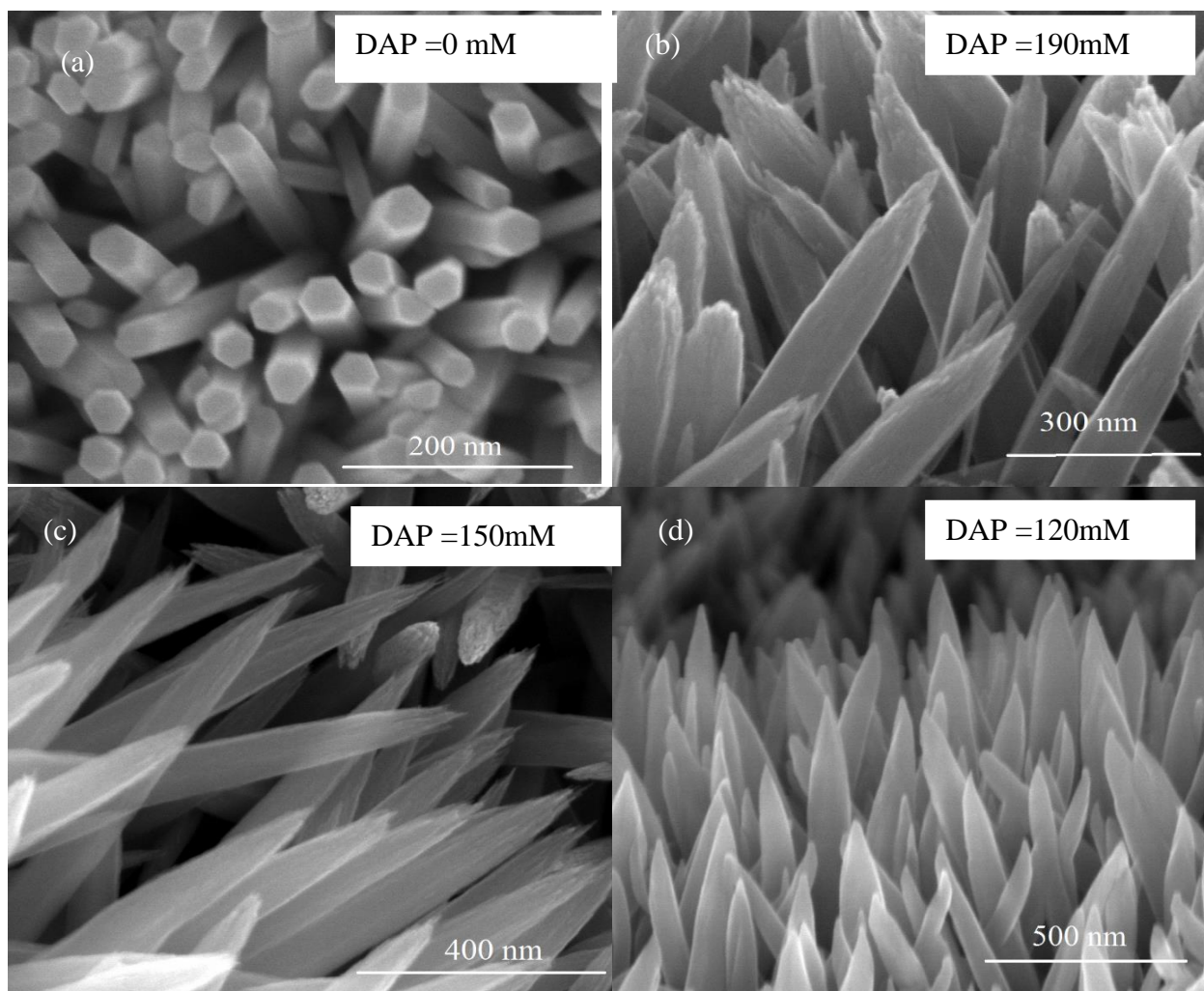


Figure 2.5 Nanoneedles growth of ZnO for zinc nitrite hexahydrate (25 mM) and HMTA (25 mM) and varying the concentration of diaminopropane (DAP) for a) 0 mM b) 190 mM c) 150 mM and d) 120 mM at 85 °C. [44]

The ZnO nanoneedle tip diameter is controlled by increasing growth time as shown in Figure 2.6 (a) and (b). As seen from the figure, the nanoneedle tip diameter reduced due to the gradual depletion of the zinc nitrate hexahydrate precursors and also the presence of diaminopropane in the growth solution [44].

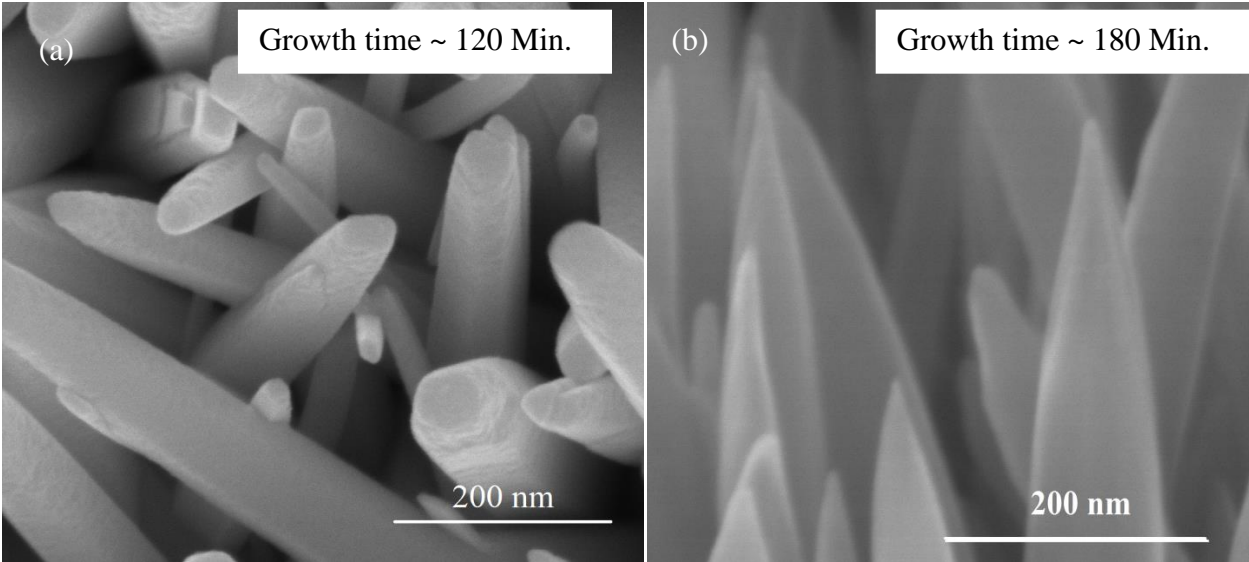


Figure 2.6 Zinc oxide nanoneedle growth for diaminopropane (DAP) 120 mM in growth solution for a) 120 min. b) 180 min. , growth temperature of 85° C. [44]

2.4 Fabrication of InAs/GaAs Quantum dots solar cells

The InAs quantum dot solar cell was grown by using a molecular beam epitaxy technique. The five periods of 2 ML InAs quantum dots/ 4 ML $\text{Al}_{0.3}\text{Ga}_{0.7}\text{As}$ / 50nm i-GaAs inserted as intrinsic region of a GaAs p-i-n solar cell. Beryllium and silicon were used for p-type and n-type dopant, respectively. The fabrication process of the InAs/GaAs quantum dot solar cell (SCs) was completed in the class 100 clean room equipped with the facilities for photolithography, wet etching, photo masking and substrate thinning. The whole fabrication process can be divided into following major steps:

2.4.1 Sample cleaning

Acetone and methanol solvents are used to remove the organic impurities from the surface by multiple cleaning steps. The rectangular size samples are first immersed in acetone for

3 minutes, rinsed with deionized (DI) water and dried with nitrogen gas. The dried samples are then immersed in methanol for 3 minutes, rinsed and dried.

2.4.2 Photolithography

In order to form 3 mm X 3 mm mesas, the sample was patterned using positive photoresist and photo mask. The cleaned samples from previous step are spin coated with AZ® P4330 positive photoresist. The coated samples are cured at 110 °C for 3 minutes and then exposed to UV light under a positive photo mask to form the square pattern. After completion of square patterning, the sample was developed using AZ® 400K developer and etched using GaAs etchant to form individual devices with an area of 0.075cm². The etch profile are characterized by using a Taylor Hobson optical profiler to measure etch depth. The etched mesas are then patterned using a second mask to form metal deposition. In order to remove oxide layer from the GaAs top surface, samples were cleaned with a diluted solution of HCl: H₂O, rinsed with DI water and dried with nitrogen.

2.4.3 Metallization and Lift off

The contact metals for both p type and n type GaAs were deposited using Angstrom Nexdep electron beam evaporator. The p-type back metal contact is formed using Au/Zn/Au deposition, while n-type front metal contact is formed using AuGe/Ni/Au deposition. The metal films were deposited under a vacuum of 2×10^{-6} Torr at a deposition rate of 0.1nm /second. During the metal deposition process the E-beam evaporator substrate was kept at 100 °C. After metallization, lift-off was performed to pattern the metal contact by immersing in acetone and agitated in an ultrasonic bath to remove the excess.

3. CHARACTERIZATION TECHNIQUES

3.1 Material Characterization

This chapter briefly discuss about the material characterization techniques used in this project. The transmission and absorbance spectra were measured using a Cary 500 UV-Vis spectrophotometer. The layer by layer deposition of antireflection structure was characterized by using Horiba LabRAM Micro-Raman spectrometer. Scanning electron microscopy (SEM) imaging was performed using Nova nanolab-250. The refractive index and reflection spectra were measured by using a J. A. Woolam VASE ellipsometer.

3.1.1 Transmission and absorbance measurements

When light is impinging on a semiconductor surface all photons with energies higher than the band gap energy are absorbed. Although within the optical bandgap some portion of the photon reflected depending on the refractive index of the material. The incident photons energy less than the optical bandgap are transmitted. An Ultraviolet-visible (UV-Vis) spectrophotometer is a device used to measure the absorbance, and transmittance. In this project a Cary 500 UV-Vis spectrophotometer was used to measure absorbance spectra of the solution phase Ta₂O₅ and ZnO nanoneedle arrays. On the other hand, a double side polished semi-insulating GaAs substrate were used in the transmission spectra measurement. The spectrometer can scan in the wavelength range of 175 nm – 3300 nm, where photomultiplier tube detector used UV-Vis region and a PbS detector for the infrared region.

3.1.2 Raman Spectroscopy

Raman spectroscopy is a commonly used information characterize the structural properties of a material like chemical composition, orientation, or crystalline quality from the phonon vibration. In Figure 3.1, the phonon vibration mechanism and inelastic Raman scattering processes for Stokes and anti-Stokes are illustrated in an energy diagram using the concept of virtual electronic states. Raman spectroscopy provides information on structural properties like chemical composition, orientation, or crystalline quality of the sample material. All this information is gathered by the analysis of the Raman signals with regard to their frequency position, frequency width, recorded intensity, and line shape in the Raman spectra. In a typical spectrum, the intensity is plotted versus the so-called Raman shift. The layer by layer deposition of antireflection structure was characterized by using Horiba LabRAM Micro-Raman spectrometer.

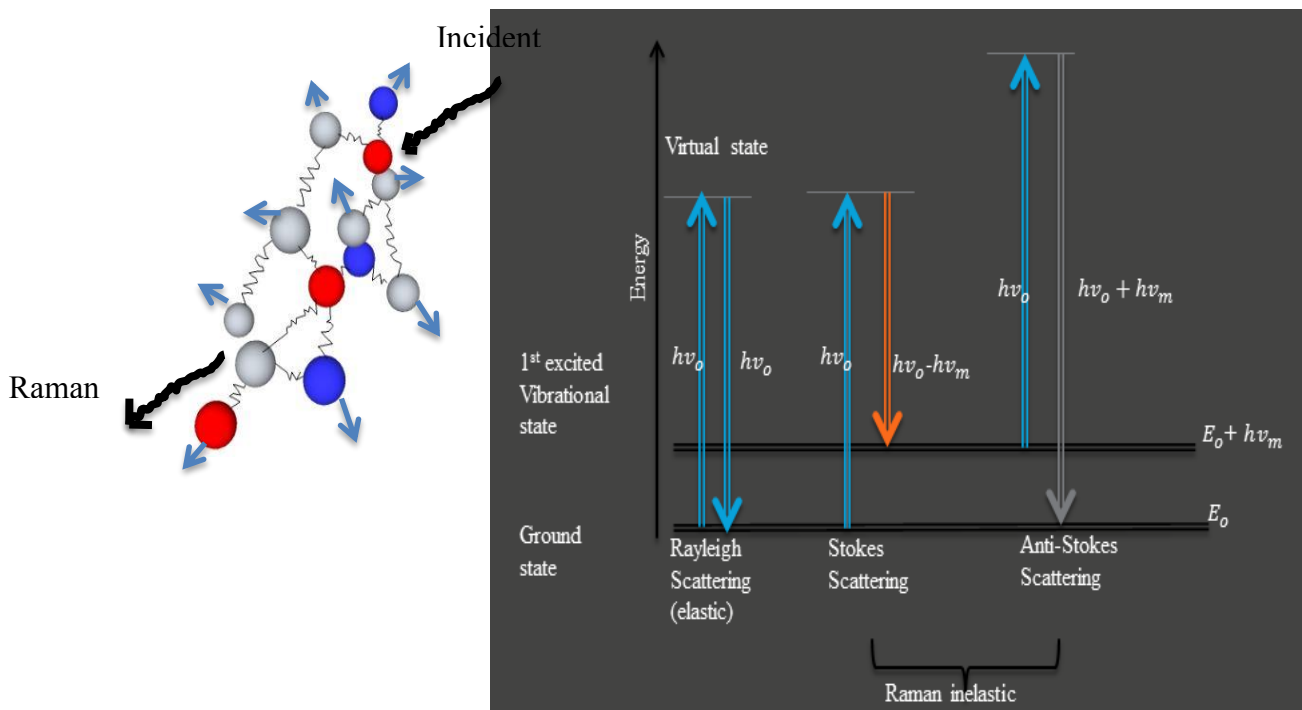


Figure. 3.1 (a) Raman molecular vibration (b) Elastic and inelastic molecular vibration

3.1.3 Spectroscopic Ellipsometry

Ellipsometry is an optical measurement technique used to investigate the refractive index, extinction coefficient, reflection and transmission spectra measurements. It uses elliptically polarized light that strikes the sample surface and the change in polarization of the reflected light from the sample is monitored. The characteristics of the polarized light reflected off the sample surface are dependent on the properties of the sample. The refractive index and reflection spectra were measured by using a J. A. Woolam VASE ellipsometer. The ellipsometer light source was adjusted to the sample with incident angles of 15°, 30°, and 60°.

3.1.4 Scanning Electron microscope (SEM)

A scanning electron microscope (SEM) produces images of a sample by scanning it with a focused beam of electrons. The impinged electrons interact with atoms in the sample and producing various signals that can be detected as information about the sample's surface topography and composition. The antireflection structures SEM imaging was performed using Nova nanolab-250 in immersion mode at 15 kV. Sample cross-sections for SEM were prepared by focused ion beam (FIB) milling on the same instrument at 30 kV.

3.2 Device Characterization

This chapter discuss about the solar cell characterization techniques used in this project. A Keithley 4200 semiconductor characterization system was used to measure I-V characteristics of the solar cells in conjunction of four sun AM 1.5 solar simulator. The spectral response

measurements were recorded by using a Bruker FS 125HR FTIR spectrometer and the external quantum efficiency measurements (EQE) were obtained by using Oriel IQE 200 spectrometer.

3.2.1 IV Characteristics measurement

A Keithley 4200 semiconductor characterization system was used to measure I-V characteristics of the solar cells in conjunction of four sun (400 mW/cm^2) AM 1.5 solar simulator. The voltage sweep is applied across the solar cell under dark and illumination condition.

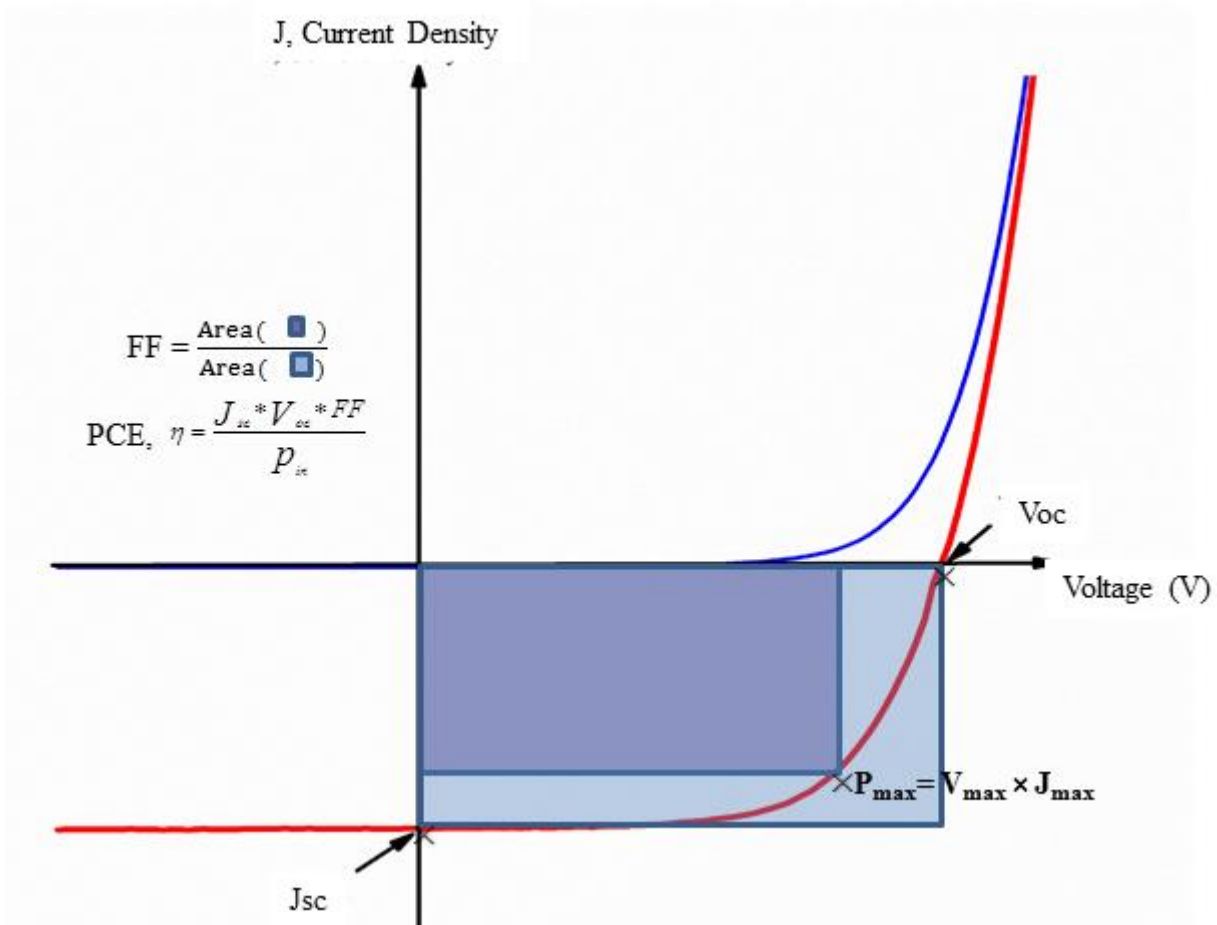


Figure 3.2. Model current density-voltage (I-V) characteristics for a solar cell in the dark (blue) and under illumination (red).

The photovoltaic performance of a solar cell is characterized with current density-voltage (I-V) characteristics. An equivalent I-V curve for a solar cell in the dark and under illumination is shown in Figure 3.2. The product of the short-circuit current density (J_{sc}), open-circuit voltage (V_{oc}), and fill factor (FF) is divided by the incident optical power to calculate the power conversion efficiency,

$$\eta = \frac{J_{sc} \times V_{oc} \times FF}{P_{in}} \quad (3.1)$$

To maximize efficiency of the solar cells, the short-circuit current density (J_{sc}), open-circuit voltage (V_{oc}), and fill factor (FF) need to be increased.

3.2.2 Quantum Efficiency

Quantum efficiency is defined as the ratio of the number of carriers generated per incident photon of particular wavelength. Generally, quantum efficiency measurements are divided into two types, external quantum efficiency (EQE) and internal quantum efficiency (IQE). EQE measurements include the optical losses like reflection and transmission while calculating the quantum efficiency of the solar cell. But IQE measurements take only the photons that are absorbed into consideration while calculating the quantum efficiency. The EQE measurements were made to characterize the solar cells by using Oriel IQE 200 spectrometer without bias illumination. An ideal solar cell the quantum efficiency curve is a square with a quantum efficiency of unity. In case of a practical solar cell the quantum efficiency is reduced due to reflection losses, front and back surface recombination. In this work, the external quantum efficiency measurements (EQE) were obtained

$$QE(\lambda) = \frac{hc}{\lambda} * \frac{s(\lambda)}{q}, \quad (3.2)$$

where, $S(\lambda)$ is the power spectral responsivity. The EQE response drops to zero below the band gap of the material.

3.2.3 Spectral Response measurement

The spectral response measurement in this project was performed by using a Bruker 125HR Fourier transform infrared (FTIR) spectrometer in conjunction with a Keithley 428 current preamplifier. A FTIR spectrometer is generally used to measure both absorption and emission spectra. It consists of a broadband light source and a detector based on the application and Michelson Interferometer which consists of a beam splitter, one fixed mirror and another movable mirror. The light reflected from the fixed and movable mirror interfere and this output of the interferometer is called the interferogram. The output changes with every position of the movable mirror, which is transformed into spatial coordinate using Fourier transform. A HeNe laser is used to track the movement of the movable mirror. The solar cells were used as the detector mounted on a cryostat. The sample chamber pressure was maintained at $\sim 10^{-6}$ Torr during the measurements. Similar to quantum efficiency, the spectral response curve drops to zero just below the band gap of the material. The spectral response measurement is performed in this project to confirm the improvement in the EQE.

4. RESULTS AND DISCUSSIONS

4.1 Introduction

This chapter briefly present the bilayer antireflection structure in conjunction with the device output. The material characterization by using Raman spectroscopy confirms the presence

of ZnO nanoneedle and the Ta₂O₅ layer. The UV-Vis absorbance spectra shows the antireflection structure can effectively transmit the solar spectrum in near ultraviolet, visible and near infrared region. The optical properties of antireflection structure including reflection spectra, refractive index, transmission spectra confirms the superior antireflective properties of the bilayer coating. Finally, the power conversion efficiency, EQE and spectral response enhancement of the

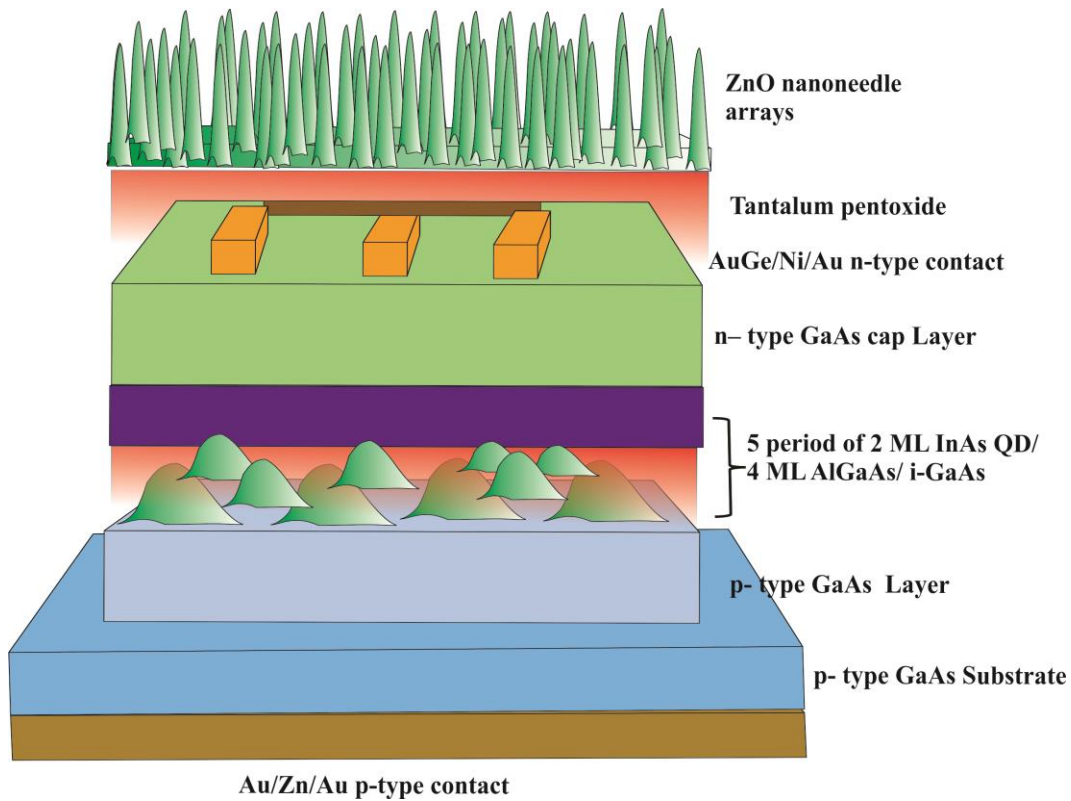


Figure 4.1. Schematic diagram of a InAs/GaAs QDs solar cell with textured surface of ZnO nanoneedle grown on planar Ta₂O₅. [44]

InAs/GaAs quantum dots solar cell due to the nanostructured bilayer antireflection coating is presented.

4.2 InAs/GaAs QDs solar cell with antireflection structure

The structure of InAs/GaAs QDs solar cell is shown in Figure 4.1. In order to compensate the reflection from the GaAs top surface, a novel antireflection structure which consists of a

Ta₂O₅ layer and ZnO nanoneedle arrays is utilized as a bilayer antireflection coating. The hierarchical surface texturing of Ta₂O₅ layer and ZnO nanoneedle arrays is shown in Figure 4.2 (a). The SEM images reveals the average length of the ZnO nanoneedle to be about 1.2 μm and tapered dimension on a 90 nm thick Ta₂O₅ layer. The pH and growth time were adjusted in order to obtain the tapered dimension. The ZnO nanoneedle tip diameter is controlled by concentration of pH and increasing the growth time as shown in experimental section of Figure 2.5 and Figure 2.6. The area density (d_A) and tip diameter of nanoneedle

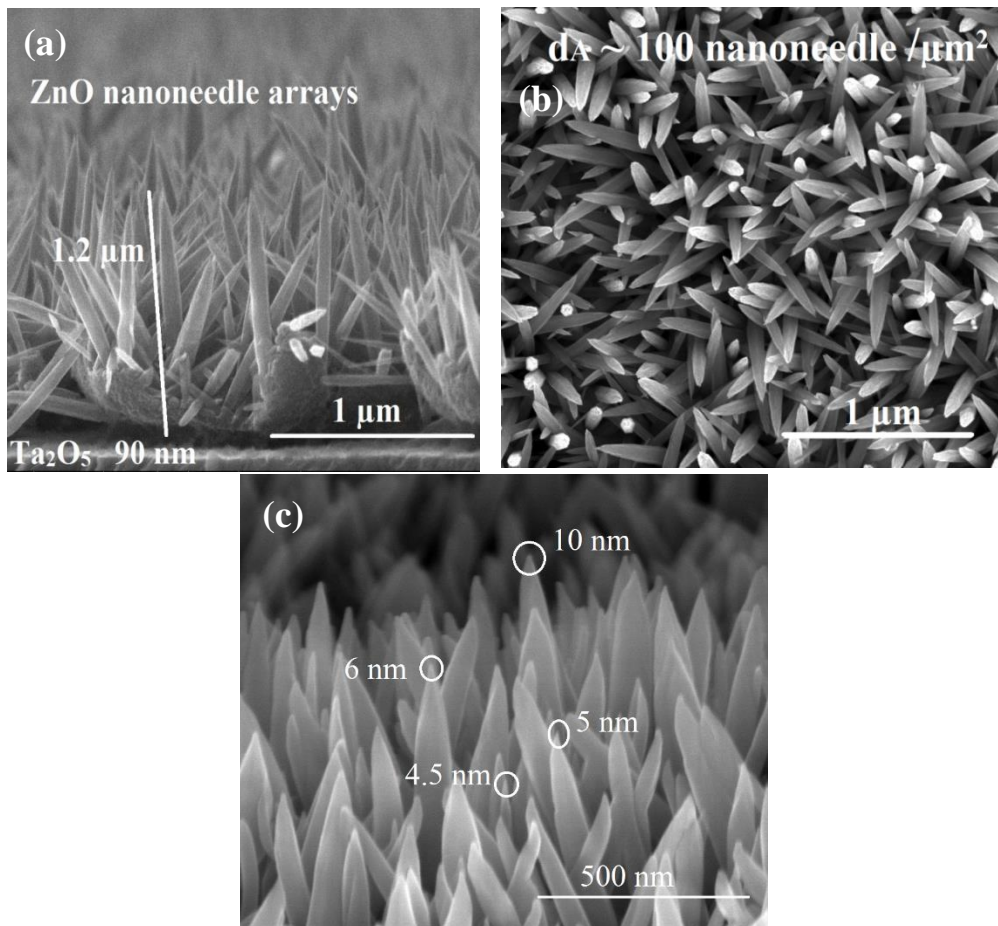


Figure 4.2. (a) and (b) A representative cross-section and top view of ZnO nanoneedles grown on top of Ta₂O₅ with scale bar of 1 μm. (c) Scanning electron microscopy (SEM) images of ZnO nanoneedle grown for diaminopropane (DAP) 120 mM in growth solution for 180 min, growth temperature of 85° C with scale bar of 500 nm resolution. [44]

arrays estimated of 100 nanoneedles/ μm^2 and 5–10 nm are shown in Figure 4(b) and (c), respectively. As seen from the figure, the nanoneedle tip diameter reduced due to the gradual depletion of the zinc nitrate hexahydrate precursors and also the presence of diamminopropane in the growth solution. The SEM images clearly show tapered shape ZnO nanoneedle structure, which is preferable for solar cell ARC applications compared to a rod like shape due to a graded refractive index effect [19,22,28].

4.2.1 Antireflection structure characterization

The layer by layer deposition of antireflection structure was characterized by using Raman spectroscopy. The Raman spectrum of Ta_2O_5 obtained by sol-gel spin coating on a cleaned glass

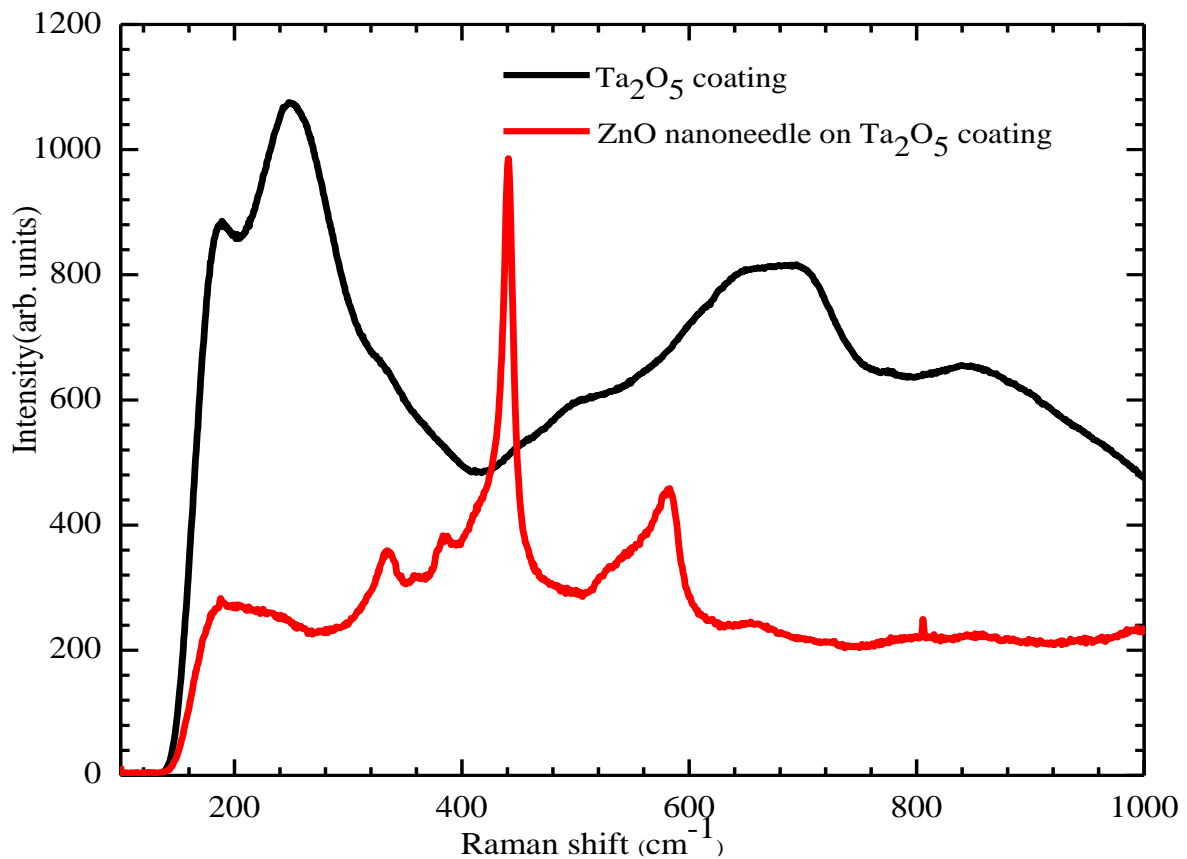


Figure 4.3. Raman spectra of sol-gel derived Ta_2O_5 film, and hydrothermally grown ZnO nanoneedles on Ta_2O_5 film measured at room temperature. [44]

slide and baked at 150 °C in ambient air is shown in Figure 4.3. The observed peaks at lower wavelength of 190 cm^{-1} , 252 cm^{-1} , and 335 cm^{-1} are attributed to Ta-O-Ta (skeletal modes) vibration. The observed peaks at higher wavelength of 510 cm^{-1} , 680 cm^{-1} , 845 cm^{-1} for the terminal modes O-Ta-O vibration, since Ta is heavier than O [38]. The Raman spectra confirm the presence of Ta_2O_5 , which contains different types of Ta-O-Ta bonding in the polyhedral structure. In contrast, the Raman mode of Ta_2O_5 disappeared after the deposition of ZnO nanoneedle arrays. The absence of Raman mode of Ta_2O_5 can be attributed to the higher length of ZnO nanoneedle arrays compared to thin Ta_2O_5 layer. The ZnO nanoneedle arrays grown on Ta_2O_5 layer shows four prominent bands at 335, 383, 440, and 583 cm^{-1} are in good agreement with the wurtzite ZnO structure [39].

The bandgap of the sol-gel grown Ta_2O_5 layer and hydrothermally grown ZnO nanoneedles

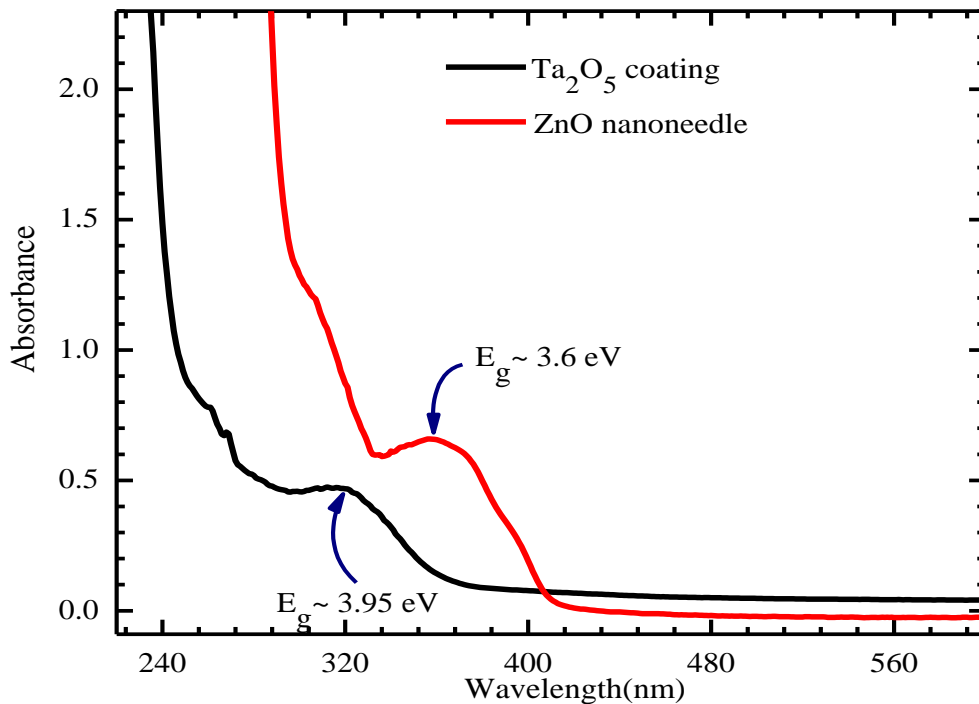


Figure 4.4. Absorbance spectra of solution phase Ta_2O_5 and ZnO nanoneedle measured and compared in wavelength range of 250 – 800nm. [44]

are measured from the absorption peak observed at 315 nm and 345 nm, respectively, as shown in Figure 4.4. The absorbance spectra of Ta₂O₅ and ZnO nanoneedle indicate the bandgap of around 3.95 eV and 3.6 eV, respectively, which are transparent in the solar cell working spectral region of $\lambda > 350$ nm [44].

4.2.2 Refractive index measurements

The refractive index of bare GaAs substrate, Ta₂O₅, and ZnO planar coating measured between 400– 870nm, are shown in Figure 4.5. The refractive index of GaAs at 650 nm is ~ 3.7 and that of the Ta₂O₅ film is ~ 1.90 . The refractive index of planar ZnO coating is ~ 1.7 measured for filling factor (the ratio of the area covered by nanoneedle arrays to the total substrate) of 1. The surface morphology of ZnO nanoneedle arrays with shrinking effective volume to top surface gradually changes the refractive index according to the effective medium theory [27, 40]

$$n_{eff} = \sqrt{n_{ZnO}^2 f + n_{air}^2 (1 - f)} , \quad (4.1)$$

Where f is a filling factor depending on the growth direction, and $n_{ZnO} \sim 1.7$ is the refractive index of ZnO layer corresponding to a filling factor of $f = 1$. The effective refractive index (n_{eff}) of ZnO nanoneedle arrays gradually reduced from 1.7 at the bottom to ~ 1.2 at the top of the nanoneedles with a filling factor of $f \sim 0.2$. As the filling factor of ZnO nanoneedle decreases from the bottom to the top, the refractive index smoothly changes toward the air [44]. In other words, the surface morphology of ZnO nanoneedle coupled with Ta₂O₅ ($n \sim 1.9$) can play a key role in suppressing the reflection by gradual reduction of refractive index away from the GaAs substrate.

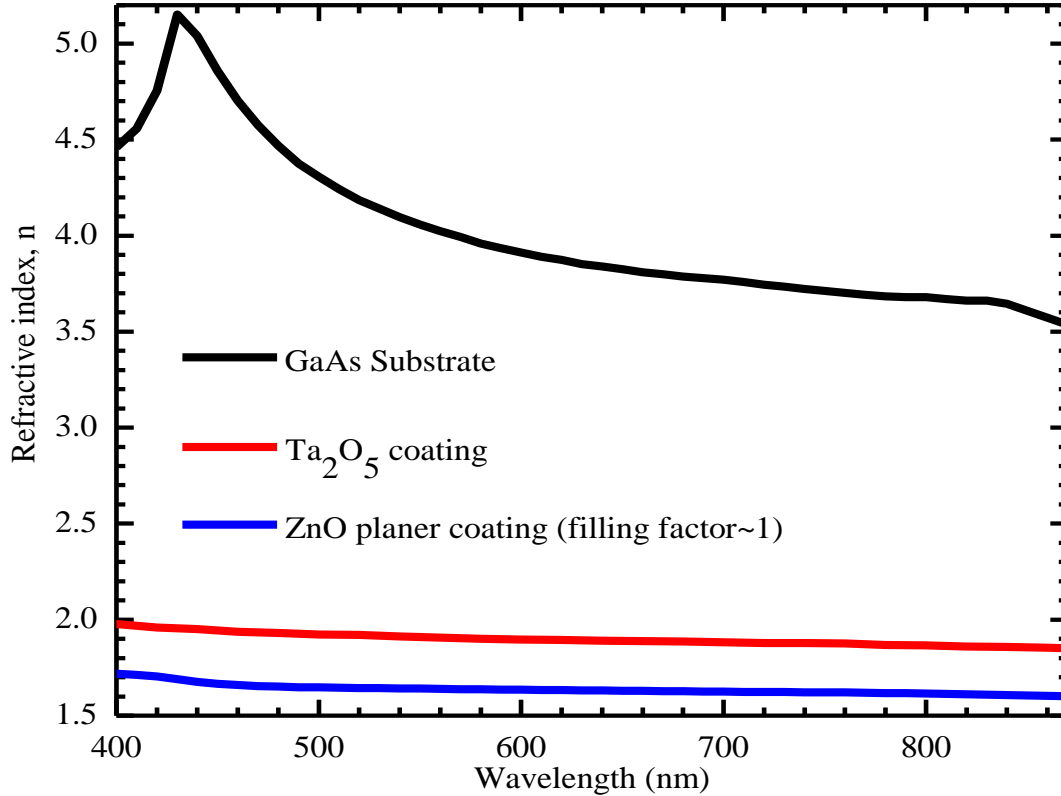


Figure 4.5. Refractive index spectra of GaAs, Ta₂O₅ layer, and ZnO planar coating compared over a range from 400 nm to 870 nm. [44]

4.2.3 Reflection and Transmission spectra measurements

While the incident sunlight impinges on the solar cell from different directions during the day, an omnidirectional ARC is desirable over wide angles of incidence. The omnidirectional and broadband antireflection characteristics of a single layer and a bilayer coating on GaAs substrate compared for angles of incidence from 15° to 60° are shown in Figure 4.6. The average reflectance of the bare GaAs substrate was measured around 35 %. A 90 nm thickness of Ta₂O₅ layer was chosen, which is around quarter wavelength thickness for a refractive index of 1.9 according to [22] $d = \lambda_{\min} / 4n_{ARC}$, where $\lambda_{\min} \sim 680\text{nm}$ is the wavelength at the minimum reflection, n_{ARC} and d are the refractive index and thickness, respectively. From the reflection

spectra, a single layer Ta₂O₅ coating suppresses the reflection to about 3 % for a single wavelength at the angle of incidence of 15°.

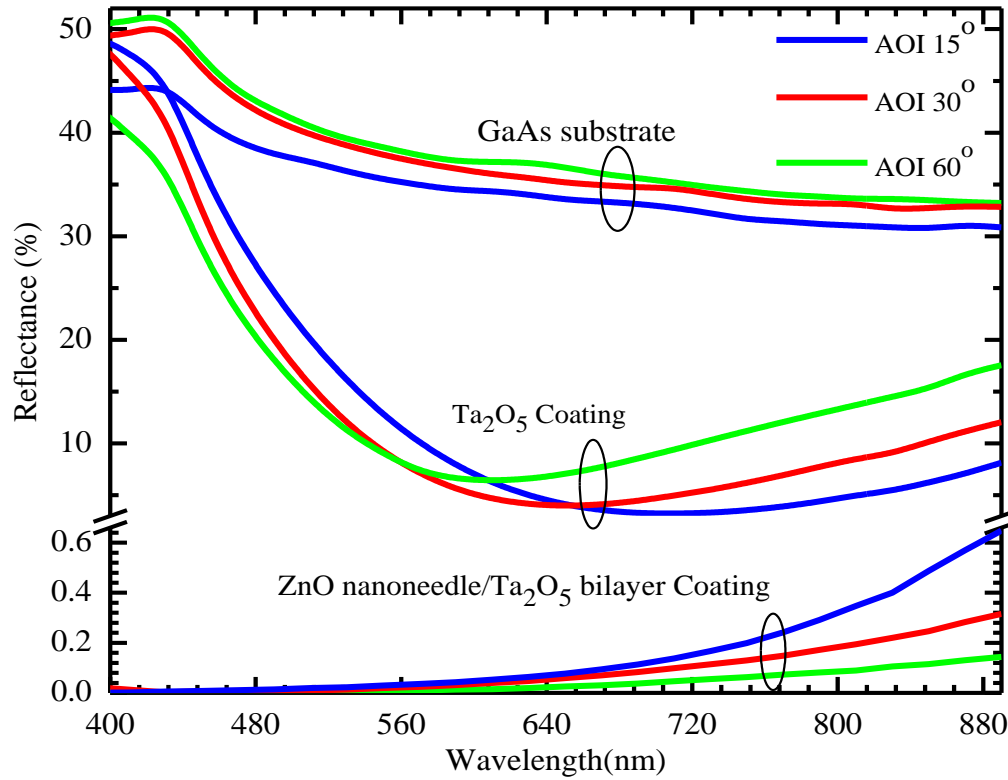


Figure 4.6. Reflectance spectra as a function of angle of incidence for GaAs substrate with pristine, Ta₂O₅, and ZnO nanoneedles surfaces. [44]

The reflection minima show blue-shift at large incidence angles since the Ta₂O₅ coating layer behaves optically thinner than 90 nm. On the other hand, the average reflectance of ZnO nanoneedle on top of Ta₂O₅ layer is less than 0.6 % over a broad spectral range and shows insensitivity to the angle of incidence.

The tapered nanoneedles coupled with Ta₂O₅ predominantly suppress the reflection due to a gradual reduction of refractive index. In other words, the ARC performance strongly depends on the nanoneedle tip diameter and the presence of the high refractive index layer of

Ta₂O₅ in order to suppress the reflection for broadband spectral range as shown in Figure 4.7. The weighted average reflectance defined as [41]

$$R_{av} = \frac{1}{\Delta\lambda} \int_{\lambda_{min}}^{\lambda_{max}} R(\lambda) d\lambda, \quad (4.2)$$

Where $R(\lambda)$ is the wavelength dependent reflectance, resulting in a R_{av} of 10 %, 2 %, and 0.5 % for ZnO nanoneedle only and bilayer coating of ZnO nanoneedle/Ta₂O₅ with non-tapered and tapered shape respectively. The reflection spectra clearly demonstrate that the hierarchical ZnO nanoneedle arrays on Ta₂O₅ coating can suppress the undesired reflection for a wide range of wavelength and angle of incidence [44].

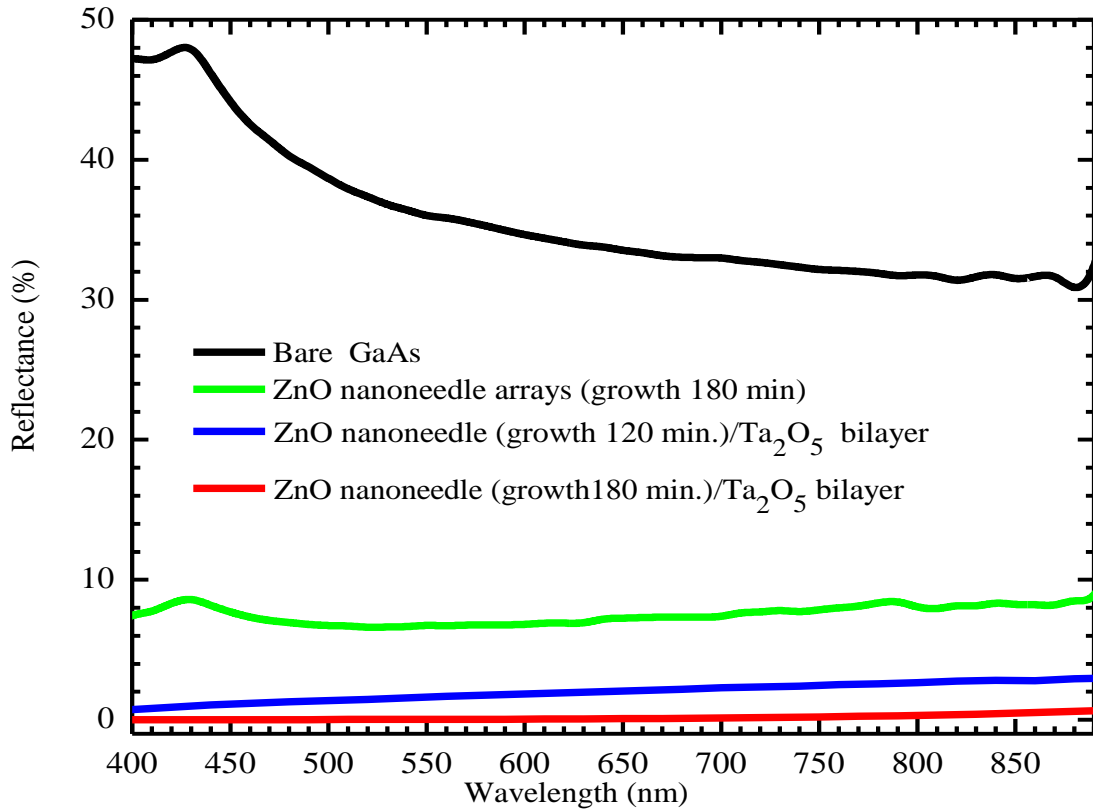


Figure 4.7. Effect of ZnO nanoneedle growth time on specular reflectance spectra for ZnO nanoneedle only (green), bilayer coating of ZnO nanoneedle/Ta₂O₅, where nanoneedle growth time for 120 minute (blue) and 180 minute (red). [44]

In order to confirm the anti-reflective properties of the bi-layer coating, the antireflection structure was coated on undoped GaAs and the transmission was measured using a UV-Vis spectrophotometer. The transmission spectra were measured in the wavelength region between 800 – 2400 nm and are shown in Figure 4.8. The average transmission of pristine GaAs is around ~53 % in the measured wavelength range. In the same wavelength range the transmission of

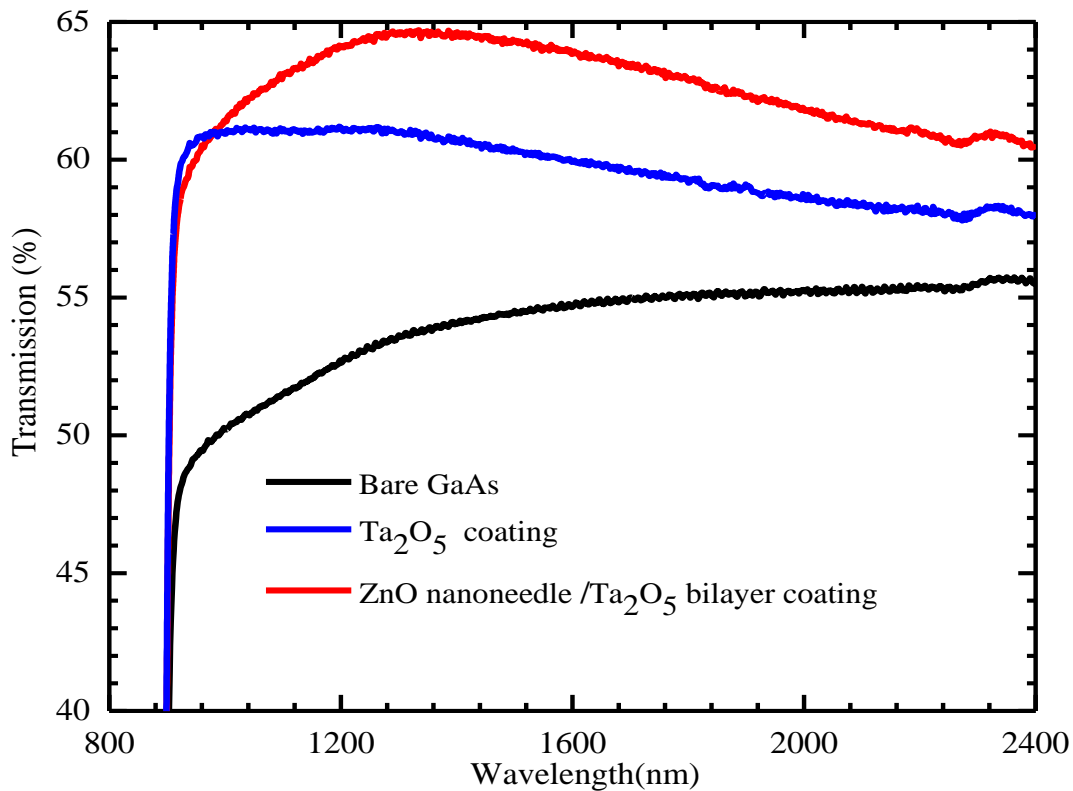


Figure 4.8. Transmission spectra measured for the GaAs substrate with pristine, Ta₂O₅, and ZnO nanoneedles surfaces. [44]

GaAs with Ta₂O₅ film is around ~61%. The transmission spectra reached their maximum of 65 % for the bilayer coating compared to the pristine GaAs substrate of 53 %. The sharp drop around 870 nm is due to the band edge of the GaAs substrate. The transmission spectra confirm an increase in photon transmission through the GaAs substrate when ZnO nanoneedles/Ta₂O₅ bilayer coating is coupled to it [44].

4.2.4 InAs/GaAs quantum dots solar cell device output

The I-V characteristics of a single layer and a bilayer antireflection coatings on InAs/GaAs QDs solar cells were measured using a four sun AM 1.5 solar simulator [44]. As seen in the Figure 4.9, a single layer Ta₂O₅ coating increased the power conversion efficiency (η) on the order of 30% from 7.10 % to 9.20 %. On the other hand, ZnO nanoneedle coupled with Ta₂O₅

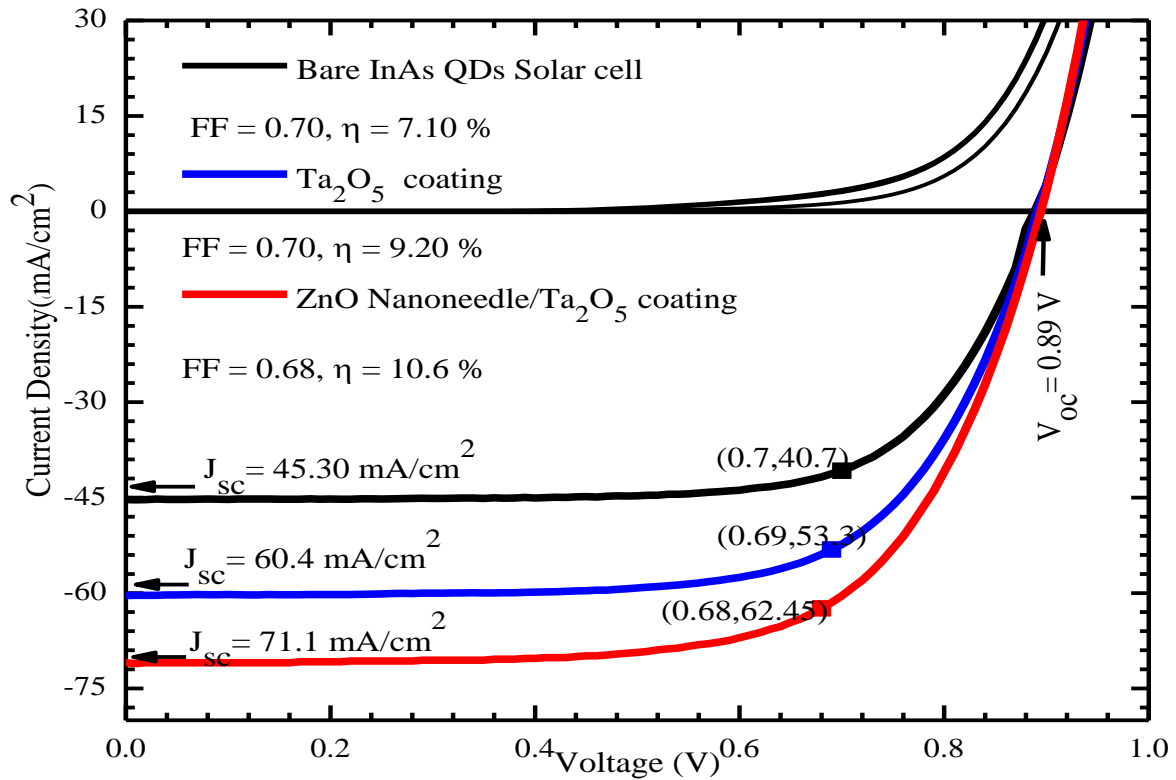


Figure 4.9. The I-V characteristics measured for the InAs/GaAs QDs solar cell with pristine, Ta₂O₅, and ZnO nanoneedles surfaces. [44]

bilayer coating showed η enhancement on the order of 50 % from 7.10 % to 10.6 %. No enhancement was observed in the open circuit voltage ($V_{oc} = 0.89$ V), thus the solar cell η enhancement was due to the increase in the generated photocurrent, which was evident from the

short circuit current density (J_{sc}) enhancement of 55 % from 45.30 mA/cm² to 71.1 mA/cm². The fill factor (FF) decreased from 0.70 to 0.68 after the bilayer coating, which indicates the junction of the solar cell slightly degrade due to the presence of a high pH (~ 12) of ZnO nanoneedle growth solution.

The EQE measured between 380- 1000 nm is shown in Figure 4.10. The EQE of the InAs/GaAs QDs solar cell coated with single layer Ta₂O₅ coating showed highest enhancement

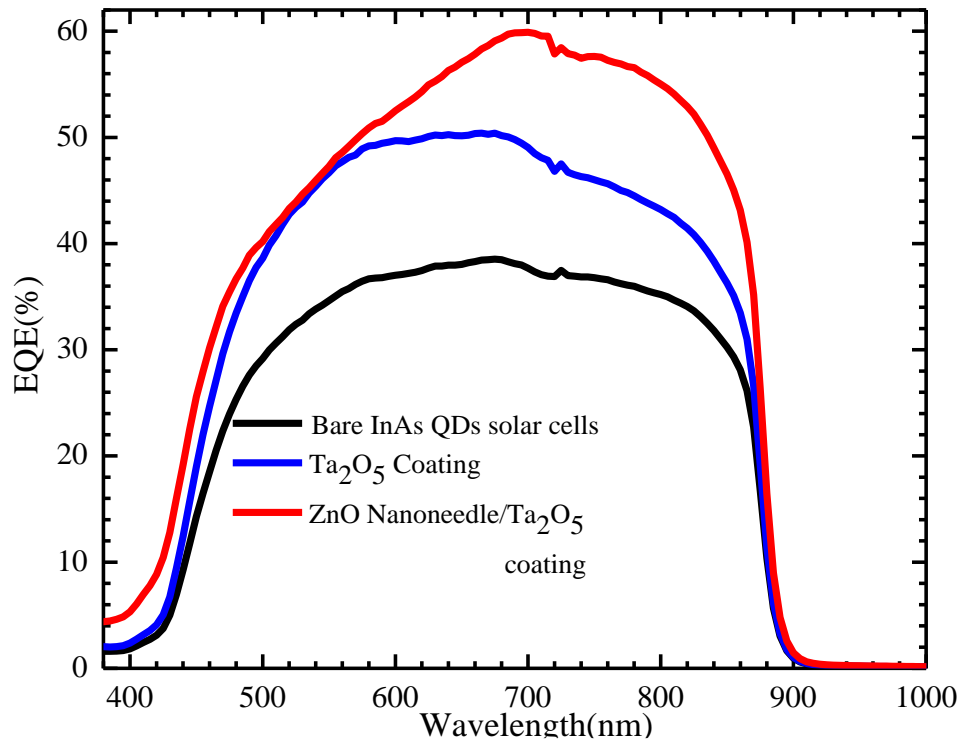


Figure 4.10. The external quantum efficiency measured for the InAs/GaAs QDs solar cell with pristine, Ta₂O₅, and ZnO nanoneedles surfaces. [44]

on the order of 30 % at 600 -750 nm range, consistent with the reduced reflectance at the same wavelength range [44]. The ZnO nanoneedle/Ta₂O₅ bilayer coating enhance the average EQE on the order of 60 % over the measured spectral range. The significant enhancement in the EQE with a bilayer coating was due to the higher generated photocurrent, originates from the

suppression of reflectance to less than 1 %. The spectral response measurement shown in Figure 4.11, also confirmed the enhancement of the EQE. The solar cell coated with single layer and bilayer coating enhanced the average spectral response on the order of 30 % and 50 %, respectively, in the 400 – 875 nm wavelength range. The rapid decrease in the response below 800 nm is due to the response of the beam splitter in the spectrometer setup.

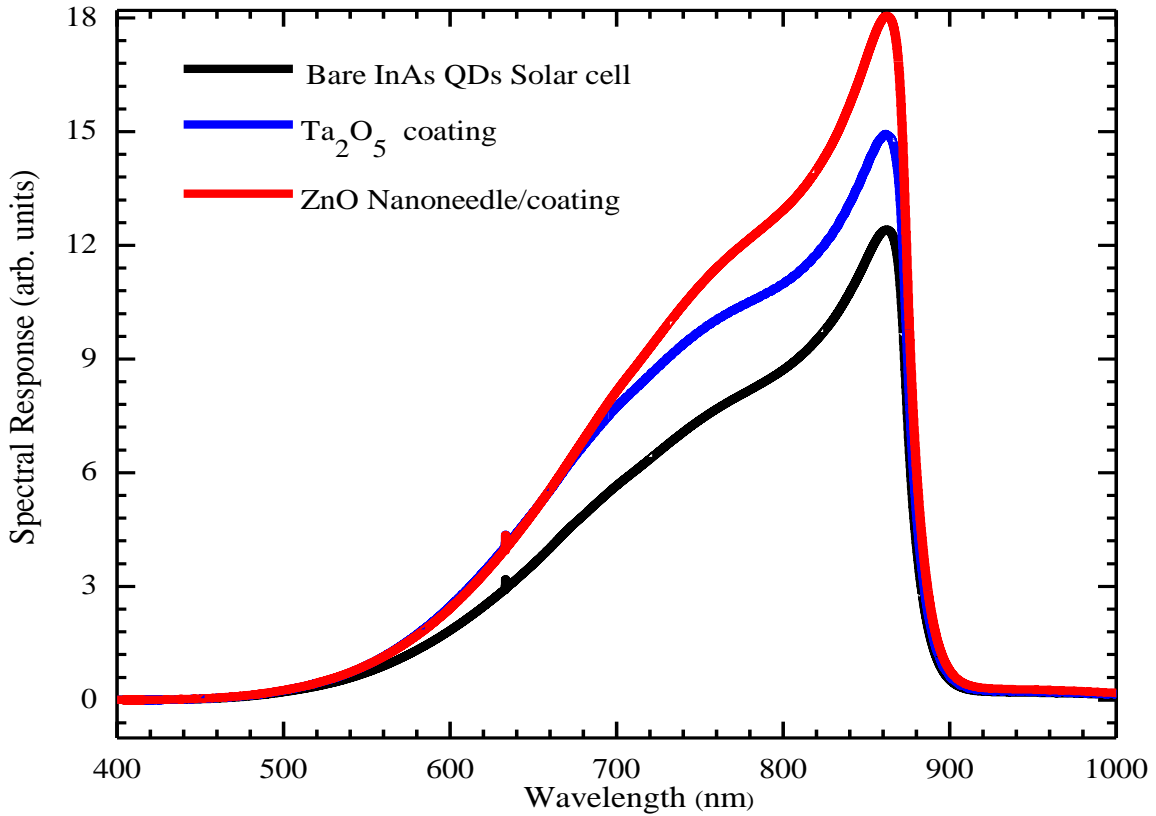


Figure 4.11. The external quantum efficiency measured for the InAs/GaAs QDs solar cell with pristine, Ta₂O₅, and ZnO nanoneedles surfaces. [44]

4.3 Discussions

The power conversion efficiency of the solar cell enhanced for several reasons. First, the hierarchical surface texturing with high to low refractive index gradient combined with planar Ta₂O₅ coating and ZnO nanoneedle bilayer ARC, increased optical transmission through the

device. The specular reflection less than 1 % and the absence of interference fringes in reflection and transmission spectra confirmed the superior antireflective properties of the bilayer coating. Second, introduction of Ta₂O₅ with refractive index of 1.9, which is an ideal single layer ARC for GaAs, is given by [42] $\sqrt{n_{GaAs} \times n_{air}}$. Third, the tapered shape ZnO nanoneedle leads to a gradual decrease of the refractive index from ZnO to air through moth-eye effect [17,19,22,27,40].

Table 1. Device characteristics comparison of GaAs based solar cells with different surface texturing.

Textured AR layers	$\overline{R_f}^{a)}$	$\frac{\Delta J_{sc}^{b)}$ $J_{sc}(\text{Bare})}$ [%]	$\frac{\Delta \eta^{c)}$ $\eta(\text{Bare})}$ [%]	$\frac{\Delta EQE_{max}^{d)}$ $\Delta EQE_{max}(\text{Bare})}$ [%]	Reference
Ta ₂ O ₅ /ZnO nanoneedle	< 1 %	52	~50	~ 60	Present work [44]
Si ₃ N ₄ /SiO ₂ /ZnO NRA	< 3 %	16	~32	~ 45	Yeh <i>et al.</i> ^[19]
TiO ₂ /nanoporous SiO ₂	< 3%	34.4	~35		Yan <i>et al.</i> ^[26]
ITO nanocolumn	< 6 %	18	~28	~ 33	Yu. <i>et al.</i> ^[20]
AZO/ZnO nanoneedle	< 12	16.7	~25	~30	Wu. <i>et al.</i> ^[27]

^{a)} $\overline{R_f}$ = Average reflection ; ^{b)} $\Delta J_{sc} = J_{sc}(\text{with ARC}) - J_{sc}(\text{Bare})$; ^{c)} $\Delta \eta = \eta(\text{with ARC}) - \eta(\text{Bare})$; ^{d)} $\Delta EQE_{max} = EQE_{max}(\text{with ARC}) - EQE_{max}(\text{Bare})$.

The effective refractive index (n_{eff}) of the nanoneedle arrays decreases as the area of the nanostructure is reduced from bottom to tapered shape top surface. The tapered shape is attributed to the gradual depletion of the zinc nitrate hexahydrate precursors and high pH (~12) due to the presence of diaminopropane in the growth solution. Fourth, the band edge of both Ta₂O₅ ($E_g \sim 3.95$ eV) and ZnO nanoneedle ($E_g \sim 3.6$ eV) are less than 350 nm, which can

effectively transmit the solar spectrum in near ultraviolet, visible and near infrared region. The overall performance enhancement obtained by using ZnO nanoneedle/ Ta₂O₅ bilayer coating is better than the performance reported [19,20,26,27] by using different combination of nanostructured surface texturing schemes on GaAs based solar cells as shown in Table 1. The significant enhancement compared to other surface texturing approach predominantly originates from the increased photon transmission by the subwavelength dimension ZnO nanoneedle geometry and coupling to a single quarter wavelength Ta₂O₅ coating. The increase in photon transmission leads to a further excitation of electron that increases the generation rate of the photo-excited charge carriers [44].

5. CONCLUSION AND FUTURE WORK

5.1 Conclusion

In conclusion, the efficiency enhancement due to a bilayer layer ZnO nanoneedle/ Ta₂O₅ antireflection coating was investigated on InAs/GaAs QDs solar cells by employing I-V, EQE, and spectral response measurements. A modified sol-gel synthesis of Ta₂O₅ was developed and the layer thickness was optimized to minimize the reflection at a single wavelength. By controlling the pH of the growth solution, tapered ZnO nanoneedle were obtained in order to provide a graded refractive index effect. The present antireflection structure played a key role in suppressions the reflection for broadband spectral range. The bilayer coating results in a on the order of 50 % power conversion efficiency enhancement of the InAs/GaAs QDs solar cell. The enhancements in the device performance were attributed to the increased photon transmission by the subwavelength dimension of ZnO nanoneedle structure that was coupled to a single quarter wavelength Ta₂O₅coating layer. The presented bilayer structure and fabrication technique for

antireflection coating is inexpensive as compared to other techniques such as sputtering, e-beam evaporation, and thus can be implemented in mass production in the photovoltaic industry.

5.2 Future Work

In this thesis, the efficiency enhancement due a bilayer of ZnO nanoneedle arrays coupled with tantalum pentoxide is presented on planar surface of InAs/GaAs quantum dots solar cells. The bilayer surface texturing approach can be replace by an in-situ bottom up tantalum pentoxide nanowire arrays. Taking advantage of the tantalum pentoxide nanostructure array will also provide the gradual variation of refractive index in order to suppress the incident photon reflection. The hydrothermal deposition of tantalum pentoxide is still challenging to grow the nanostructure arrays [43]. But the precise control of the synthesis condition may led to a successful antireflection light trapping scheme of tantalum pentoxide nanowire. Also, replacing the planar GaAs top surface by a microgroove surface with nanostructure ARC also may improve the solar cell performance.

REFERENCES

- [1] X. Sheng, L. Shen, T. Kim, L. Li, X. Wang, R. Dowdy, P. Froeter, K. Shigeta, X. Li, R. G. Nuzzo, N. C. Giebink, J. A. Rogers, “Doubling the Power Output of Bifacial Thin-Film GaAs Solar Cells by Embedding Them in Luminescent Waveguides” *Adv. Energy Mater.*, vol. 3, pp. 991-996, Aug. 2013.
- [2] J. Jean , S. Chang , P. R. Brown , J. J. Cheng , P. H. Rekemeyer , M. G. Bawendi , S. Gradečak, and V. Bulovic, “ZnO nanowire arrays for enhanced photocurrent in PbS quantum dot solar cells” *Adv. Mater.*, vol 25, pp. 2790-2796, Mar. 2013.
- [3] D. Shahrjerdi, S. W. Bedell, C. Bayram, C. C. Lubguban, K. Fogel, P. Lauro, J. A. Ott, M. Hopstaken, M. Gayness, D. Sadana, “Ultralight High-Efficiency Flexible InGaP/(In)GaAs Tandem Solar Cells on Plastic” *Adv. Energy Mater.*, vol. 3, pp. 566-571, May 2013.
- [4] A. Luque and A. Marti, “Increasing the Efficiency of Ideal Solar Cells by Photon Induced Transitions at Intermediate Levels” *Phys. Rev. Lett.*, vol. 78, pp. 5014-5017, June 1997.
- [5] D. Alonso-Álvarez, A. G. Taboada, J. M. Ripalda, B. Alén, Y. González, L. González, J. M. García, F. Briones, A. Martí, A. Luque, A. M. Sánchez, and S. I. Molina, “Carrier recombination effects in strain compensated quantum dot stacks embedded in solar cells” *Appl. Phys. Lett.*, vol. 93, pp. 123114- 123114-3, Sep. 2008.
- [6] C. Yeo, J. H. Kwon, S. J. Jang, Y. T. Lee, “Antireflective disordered subwavelength structure on GaAs using spin-coated Ag ink mask” *Opt. Express*, vol. 20, pp. 19554-19562, Aug. 2012.
- [7] L. Diedenhofen , G. Grzela , E. Haverkamp , G. Bauhuis ,J. Schermer , J. G. Rivas , “Broadband and omnidirectional anti-reflection layer for III/V multi-junction solar cells” *Sol. Energy Mater. Sol. Cells* ,vol. 101, pp. 308-314, Mar. 2012.
- [8] D. Zhou, G. Sharma, S. F. Thomassen, T. W. Reenaas, and B. O. Fimland, “Positioning effects on quantum dot solar cells grown by molecular beam epitaxy” *Appl. Phys. Lett.*, vol. 96, pp.083108- 083108-3, Feb. 2010.
- [9] S. M. Hubbard, C. D. Cress, C. G. Bailey, R. P. Raffaele, S. G. Bailey, and D. M. Wilt, “Effect of strain compensation on quantum dot enhanced GaAs solar cells” *Appl. Phys. Lett.*, vol. 92, pp. 123512-123512-3, Mar. 2008.
- [10] G. Wei and S. R. Forrest, “Intermediate-Band Solar Cells Employing Quantum Dots Embedded in an Energy Fence Barrier” *Nano Lett.*, vol. 7, pp. 218-222, Jan. 2007.

- [11] M. Victoria, C. Domínguez, I. Antón, G.Sala, “Antireflective coatings for multijunction solar cells under wide-angle ray bundles” *Opt. Express.*, vol 20, pp. 8136-8147, March 2012.
- [12] S. Chhajed, D. J. Poxson, Xing Yan, J Cho, E. F. Schubert,R. E. Welser, A. K. Sood, and Jong Kyu Kim "Nanostructured Multilayer Tailored-Refractive-Index Antireflection Coating for Glass with Broadband and Omnidirectional Characteristics" *Appl. Phys. Express*, vol. 4, pp. 052503, May 2011.
- [13] S. L. Diedenhofen, G. Vecchi, R. E. Algra, A. Hartsuiker, O. L. Muskens, G. Immink, E. P. A. M. Bakkers, W. L. Vos and J. G. Rivas, “Broad-band and Omnidirectional Antireflection Coatings Based on Semiconductor Nanorods” *Adv. Mater.*,vol. 21, pp. 973-978, Mar. 2009.
- [14] Y. F. Huang , S. Chattopadhyay , Y. J. Jen , C. Y. Peng , T. A. Liu ,Y. K. Hsu , C. L. Pan ,H.C. Lo, C. H. Hsu,Y. H. Chang, “Improved broadband and quasi-omnidirectional anti-reflection properties with biomimetic silicon nanostructures” *Nat. Nanotechnol.*, vol. 2, pp. 770-774, Dec. 2007.
- [15] Y. M. Song, S. J. Jang, J. S. Yu, and Y. T. Lee, “Bio-inspired parabola subwavelength structures for improved broadband antireflection” *Small*, vol. 6, pp. 984-987, May 2010.
- [16] J. Q Xi, M F Schubert, J K Kim, E F Schubert, M Chen, S-Y Lin, W. Liu,J. A. Smart, “Optical thin-film materials with low refractive index for broadband elimination of Fresnel reflection” *Nat. Photonics*, vol. 1,pp. 176-179, Mar. 2007.
- [17] Q. Chen , G. Hubbard , P. A. Shields , C. Liu , D. W. E. Allsopp ,W. N. Wang , S. Abbott , “Broadband moth-eye antireflection coatings fabricated by low-cost nanoimprinting” *Appl. Phys. Lett.*, vol. 94, pp. 263118-263118-3, Jun. 2009.
- [18] J. Tommila , V. Polojärvi , A. Aho , A. Tukiainen , J. Viheriälä , J. Salmi ,A. Schramm , JM Kontio , A. Turtiainen , T. Niemi ,”Nanostructured broadband antireflection coatings on AlInP fabricated by nanoimprint lithography” *Sol. Energy Mater. Sol. Cells*, vol. 94, pp. 1845-1848, Oct. 2010.
- [19] L. Yeh, K. Lai, G. Lin, P. Fu, H. Chang,C. Lin,J. He,”Giant Efficiency Enhancement of GaAs Solar Cells with Graded Antireflection Layers Based on Syringelike ZnO Nanorod Arrays” *Adv. Energy Mater.*, vol. 1,pp. 506-510, July 2011.
- [20] P. C. Yu, C. H. Chang, C. H. Chiu, C. S. Yang, J. C. Yu, H. C. Kuo, S. H. Hsu and Y. C. Chang, “Efficiency Enhancement of GaAs Photovoltaics Employing Antireflective Indium Tin Oxide Nanocolumns” *Adv. Mater.*, vol. 21,pp. 1618-1621, April 2009.
- [21] Y-C Chao, C-Y Chen, C-A Lin, Y-A Dai, J-H He,”Antireflection effect of ZnO nanorod arrays” *J. Mater. Chem.*, vol. 20, pp. 8134-8138, Aug. 2010

- [22] Y. J. Lee , D. S. Ruby , D. W. Peters , B. B. McKenzie , J. W. P. Hsu, "ZnO Nanostructures as Efficient Antireflection Layers in Solar Cells" *Nano Lett.*, vol. 8, pp. 1501-1505, April 2008.
- [23] S. A. Boden and D. M. Bagnall, "Tunable reflection minima of nanostructured antireflective surfaces" *Appl. Phys. Lett.*, vol. 93, pp. 133108-133108-3, Sep. 2008.
- [24] M. Heo, H. Cho, J. Jung, J. R. Jeong, Soojin Park, J. Y. Kim, "High-Performance Organic Optoelectronic Devices Enhanced by Surface Plasmon Resonance" *Adv. Mater.*, vol. 23, pp. 5689-5693, Dec. 2011.
- [25] M.T. Sheldon, C.N. Eisler, H. A. Atwater, "GaAs Passivation with Trioctylphosphine Sulfide for Enhanced Solar Cell Efficiency and Durability" *Adv. Energy Mater.*, vol 2, pp. 339-344, Mar. 2012.
- [26] X. Yan, D. J. Poxson, J. Cho, R. E. Welser, A. K. Sood, J. K. Kim, E. F. Schubert, "Enhanced Omnidirectional Photovoltaic Performance of Solar Cells Using Multiple-Discrete-Layer Tailored- and Low-Refractive Index Anti-Reflection Coatings" *Adv. Funct. Mater.*, vol. 23, pp. 583-590, Feb. 2013.
- [27] T. H. Wu, R. Chuang, C. Y. Huang, C. Y. Cheng, C. Y. Huang, Y. C. Lin, Y. K. Sua, "ZnO Nanoneedles/ZnO:Al Film Stack as an Anti-Reflection Layer for High Efficiency Triple Junction Solar Cell" *Electrochem. Solid State Lett.*, vol. 15, pp. H208-H210, Sep. 2012.
- [28] C. A. Lin, K. Y. Lai, W. C. Lien, J. H. He, "An efficient broadband and omnidirectional light-harvesting scheme employing a hierarchical structure based on a ZnO nanorod/Si₃N₄-coated Si microgroove on 5-inch single crystalline Si solar cells" *Nanoscale*, vol. 4, pp. 6520-6526, Aug. 2012.
- [29] Y. Tak, K. Yong, "Controlled growth of well-aligned ZnO nanorod array using a novel solution method." *J. Phys. Chem. B*, vol. 109, pp. 19263-19269, Sep. 2005.
- [30] T. J. Rehg, J. A. Tapia, A. Knoesen, B. G. Higgins, "Sol-gel derived tantalum pentoxide films as ultraviolet antireflective coatings for silicon." *Appl. Opt.*, vol. 28, pp. 5215-5221, Dec. 1989.
- [31] C. Christensen, R. Reus, and S. Bouwstra, "Tantalum oxide thin films as protective coatings for sensors" *J. Micromech. Microeng.*, vol. 9, pp. 113-118, June 1999.
- [32] N. Ozer, Y. X. He, C. M. Lampert, "Ionic conductivity of tantalum oxide films prepared by sol-gel process for electrochromic devices" *Proc. SPIE*, vol. 2255, pp. 456-466, Sep. 1994.
- [33] S. Molesky, C. J. Dewalt, Z. Jacob, "High temperature epsilon-near-zero and epsilon-near-pole metamaterial emitters for thermophotovoltaics" *Optics Express*, vol. 21, pp. A96-A110, Jan. 2013.

- [34] F. Djidjeli , E. Jaberansary, H. M. H. Chong , D. M. Bagnall, “Broadband plasmonic couplers for light trapping and waveguiding” *Proc. SPIE nanophotonics III*,vol. 7712, pp. 77122R, May 2010.
- [35] Lindmayer,Joseph, Allison,J. Frederick, “Tantalum pentoxide anti-reflective coating” *US Patent* **1975**, 3922774.
- [36] Y. Sun, P.A. Sermon, M.S.W. Vong, “Design of reflective tantala optical coatings using sol-gel chemistry with ethanoic acid catalyst and chelator” *Thin solid films.*,vol. 278,pp. 135-139, May 1996.
- [37] M.J. Wolf,S. Roitsch, J. Mayer, A. Nijmeijer , H.J.M. Bouwmeester, “Fabrication of ultrathin films of Ta₂O₅ by a sol–gel method” *Thin Solid Films.*,vol. 527,pp. 354-357, Jan. 2013.
- [38] P. S.Dobal , R. S.Katiyar, Y.Jiang, R.Guo, and A. S.Bhalla, (2000), “Raman scattering study of a phase transition in tantalum pentoxide” *J. Raman Spectrosc.*,vol. 31,pp. 1061-1065, Dec. 2000.
- [39] B. Cao,W. Cai,G.Duan,Y. Li,Q. Zhao, D. Yu, “A template-free electrochemical deposition route to ZnO nanoneedle arrays and their optical and field emission properties” *Nanotech.*,vol. 16,pp. 2567-2574, Sep. 2005
- [40] S. Kuo,M. Y. Hsieh,H. V. Han,F.I Lai, Yu-Lin Tsai,Jui-Fu Yang,T.Y. Chuange, H.C. Kuo, “Dandelion-shaped nanostructures for enhancing omnidirectional photovoltaic performance” *Nanoscale.*,vol. 5,pp. 4270-4276, May 2013.
- [41] S. Chhajed, M. F. Schubert, J. K. Kim, E. F. Schubert, Nanostructured multilayer graded-index antireflection coating for Si solar cells with broadband and omnidirectional characteristics, *Appl. Phys. Lett.*, vol. 93 , pp251108, Dec. 2008.
- [42] B. Y. Su,S.Y. Chu,Y.D. Juang,M.C. Lin,C.C. Chang,C.J Wu, “Efficiency Enhancement of GaAs Photovoltaics Due to Sol-Gel Derived Anti-Reflective AZO Films” *J. Electrochem. Soc.*,vol. 159, pp. H312-H316, Jan. 2012.
- [43] J. Duan,W. Shi,L. Xu, G. Mou, Q. Xin and J. Guan "Hierarchical nanostructures of fluorinated and naked Ta₂O₅ single crystalline nanorods: hydrothermal preparation, formation mechanism and photocatalytic activity for H₂ production" *Chem. Commun.*, vol. 48, pp. 7301–7303, May 2012.
- [44] J. C. Sarker, Y. F. Makableh, R. Vasan, S. Lee, M. O. Manasreh, M. Benamara, "Broadband Nanostructured Antireflection Coating for Enhancing InAs/GaAs Quantum Dots Solar Cells Performance", *IEEE Journal of Photovoltaic* (2014). [Under Review]

Appendix

Associated Contributions

Journal Publications

1. J. C. Sarker, Y. F. Makableh, R. Vasana, S. Lee, M. O. Manasreh, M. Benamara, "Broadband Nanostructured Antireflection Coating for Enhancing InAs/GaAs Quantum Dots Solar Cells Performance", IEEE Journal of Photovoltaic (2014). [Under Review]
2. J. C. Sarker, R. Vasana, Y. F. Makableh, S. Lee, A. I. Nusir and M. O. Manasreh, " Enhanced performance of surface modified InAs quantum dots solar cell by sol-gel grown tantalum pentoxide antireflection coating", Solar Energy materials and solar cells (2014). [Accepted]
3. Y. F. Makableh, R. Vasana, J. C. Sarker, A. Nusier, S. Seal, M. O. Manasreh "Enhanced device performance by ZnO anti-reflection coating for GaAs solar cell," Solar Energy Materials & Solar Cells 123(2014)178–182

Conferences Publications

1. R. Vasana, Y. F. M. Makableh, J. C. Sarker, M. O. Manasreh, "Enhanced Photocurrent due to Interband Transitions from InAs Quantum Dots Embedded in InGaAs Quantum Well Solar Cells," MRS- Spring 2013 proceedings, vol. 1551 (2013).
2. Y. F. Makableh, R. Vasana, J. C. Sarker, S. Lee, M. A. Khan and M. O. Manasreh, "Enhanced response in InAs quantum dot in a quantum well solar cells by anti-reflection coatings," MRS- Spring 2013 proceedings, vol. 1551 (2013)

Poster Presentation:

1. "Anisotropic nano-corrugated surface topology of ZnO/MgF₂ composite antireflection coating for GaAs solar cell by an aquatic route" Spring ASSET conference, Little rock, Arkansas, May 26, 2013.